# GIS AS A TOOL FOR STUDYING THE GEOMORPHOLOGY OF FINE-GRAINED DEPOSITS OF THE COLORADO RIVER IN GRAND CANYON NATIONAL PARK

final report
in partial fulfillment of
contract 1425-98-FC-40-22640
Grand Canyon Monitoring and Research Center

Hoda A. Sondossi and John C. Schmidt
Department of Geography and Earth Resources
Utah State University
Logan, Utah 84322-5240

March 2001

# ABSTRACT

GIS data developed from interpretation of aerial photos can be used to investigate spatial and temporal trends in the size of eddy sand bars along debris fan-affected rivers. We developed comprehensive digital records of sand bars in the reach between Lees Ferry and Badger Creek Rapid on the Colorado River as depicted on aerial photographs taken between 1935-1996. These data were analyzed and compared with data previously collected in reaches near Point Hansbrough and the LCR confluence in similar studies. Our methods proved effective in detecting temporal trends in the size distribution of eddy sand bars in a give reach; for example, the areal extent of sand bars in the study reach was not significantly affected by the closure of Glen Canyon Dam. These methods were also effective in quantitatively comparing different reaches of the river, thereby allowing the evaluation of whether longitudinal trends in sand storage actually exist. In addition to comprehensive areal data, our methods made possible quantification of topographic data through time, at a reach scale. These techniques also made possible the detection of how a single flood affected sand bars, and the longevity of these effects. For example, floods scour low-elevation portions of eddies and build high-elevation parts; these effects were not detectable six months after the flood. Modifications were made to techniques of digitizing and data analysis, that are based on similar studies conducted downstream, which increased the efficiency of the entire process.

# INTRODUCTION

Environmental monitoring is a fundamental component of many natural resource management strategies. For example, the Northwest Forest Plan developed for the northern Pacific Coast of the United States describes three types of monitoring that are essential parts of the Plan: implementation, effectiveness, and validation (Mulder et al., 1999). Environmental monitoring is a necessary part of assessing the ecological health of the nation's streams, and proposed monitoring programs include measurement of numerous physical and biological attributes (Lazorchak et al., 1998). In the case of the Colorado River in the Grand Canyon of northern Arizona, physical, biological, and cultural attributes each have inherent value, as well as comprising parts of a complex ecosystem that has been profoundly affected by Glen Canyon Dam (Schmidt et al., 1999).

One physical attribute that is of great interest is the deposits of fine sediment that occur as bars and banks. These deposits are distinctive relicts of the pre-dam landscape of the Colorado River, and the National Research Council (1996) recommended that the size and abundance of these bars be considered indicators of the degree to which the Colorado River functions like the pre-dam river. Each year approximately 20,000 river runners use sand bars as campsites. These deposits also are substrate for riparian vegetation and they create adjacent aquatic habitat utilized by certain native fish. Long-term trends in the distribution of these deposits are input variables to a comprehensive model of the Colorado River ecosystem (Korman and Walters, 1998). Thus, monitoring these deposits is an essential element of managing the Colorado River.

The purpose of this paper is to describe an environmental monitoring strategy that utilizes aerial photograph analysis and geographic information systems (GIS) so that

monitoring can be conducted over a large spatial scale, yet with precision and accuracy that is appropriate for characterizing the range of variability in size of sand bars that is inherent in the sediment transport processes of the Colorado River. Recent scientific advances are summarized in order to provide a background concerning the variability of these processes and their associated fine-grained deposits. This background is used to demonstrate that a large-scale monitoring approach is appropriate as a component of a program for monitoring fine-grained deposits along a large debris fan-affected river such as the Colorado River in Grand Canyon. We describe in detail how these data are obtained from aerial photographs, incorporated within a GIS, and subsequently analyzed. The methods are those pioneered by Schmidt and Leschin (1995), Schmidt et al. (1999), and Grams and Schmidt (1999), although we modified these methods to make them more efficient. The approach is illustrated with data collected in a study reach 25 km downstream from Glen Canyon Dam, and these data are compared with similar data available for other reaches of the Colorado River (Schmidt et al., 1999). We describe the accuracy and precision of these methods, and we show how data generated using these methods can be used to identify temporal and spatial trends in the size of fine-grained bars and banks. The comprehensive historical interpretation of these data is described elsewhere.

This draft report is one of several in partial fulfillment of contract 1425-98-FC-40-22640 with the Grand Canyon Monitoring and Research Center. This report specifically addresses aspects of work product 2 of the revised project proposal submitted by Schmidt et al. to GCMRC on October 17, 1997.

# BACKGROUND ABOUT THE COLORADO RIVER IN GRAND CANYON

The closure of Glen Canyon Dam in March 1963 affected the downstream reaches of the Colorado River in Glen Canyon National Recreation Area, Grand Canyon National Park, and lands of Hualapai Indian Reservation (figure 1). Physical and ecological changes resulted from the elimination of floods, introduction of daily fluctuations in dam releases due to hydro-power demands, trapping of all fine-grained sediment previously supplied by the upstream drainage basin, and changes in the annual thermal regime (Webb et al., 1999; Topping et al., 2000a). Physical changes included scour of the bed, increase in channel width, and increase in bed material size in the 25 km immediately downstream from the dam (Pemberton, 1976; Webb et al., 1999; Topping et al., 2000a). One notable change that occurred along the channel-margins further downstream has been the reduction in size and number of sand bars used as campsites by recreational boaters (Kearsley et al., 1994). It is essential to monitor changes in the volume of sand stored in eddies because of their importance to river management agencies and as a component of the reach sediment budget. Sand bars large enough to be used as campsites form primarily in eddies. Eddies store as much as 85% of fine-grained sediment in Grand Canyon, because eddies are efficient traps of suspended sediment (Schmidt and Rubin, 1995).

## ***Changes in sediment flux***

Sediment transport of the Colorado River in Grand Canyon National Park was greatly reduced by closure of Glen Canyon Dam; all sediment delivered from upstream is now trapped behind the dam. The post-dam annual load of suspended sediment measured just upstream from the confluence of the Paria River (USGS station 09250000, Colorado

River at Lees Ferry, Arizona) is less than 0.5% of the pre-dam era (Topping et al., 2000a). The post-dam annual load of suspended sediment, calculated downstream from the Paria River confluence, is about 5% of the pre-dam era (Topping et al., 2000a) (figure 2). The Colorado River now transports less than 20% of the amount of suspended sediment it did in the pre-dam era past the USGS gaging station located just upstream from Bright Angel Creek (USGS station 09380000, Colorado River near Grand Canyon, Arizona) which is downstream from both the Paria River and the Little Colorado River (LCR) (Topping et al., 2000a). Thus, the suspended sand, silt, and clay introduced to the mainstem by the Paria River and the LCR are the only significant inputs of fine-grained sediment for the reaches downstream.

The LCR confluence is 100 km downstream from the Paria, and concentrations of suspended sediment are greater downstream from the LCR. Thus, there is longitudinal variation in the concentrations of suspended sediment, and this variation has implications for longitudinal variation in the size of eddy bars. Schmidt (1999) showed that eddies in the reach immediately downstream from the LCR had higher deposition rates of fine sediment than eddies immediately upstream during the 1996 controlled flood, and these higher rates have the potential to produce larger sand bars (Wiele et al, 1999). Concentrations of suspended sediment were twice as great downstream from the LCR.

***Lack of understanding in the behavior of eddies in response to dam closure***

The extent of erosion of the bed following dam closure and the rate of downstream progression of this erosion are well documented in the 25 km immediately downstream from the dam (Pemberton, 1976; Burkham, 1986). Although several studies have attempted to deduce trends in storage of fine-grained sediment further downstream

(e.g. Konieczki et al., 1997; Hazel et al., 1999), the link between storage of fine sediment on the bed and in eddies is not well understood in most of Grand Canyon. Significant progress has been made by Rubin et al. (1998), Topping et al. (2000b).

***Hydrology and storage of fine-grained sediment***

In the pre-dam era, the Colorado River had two annual flood seasons, and this flow regime had the potential to produce annual variability in bar size. The late spring/early summer snowmelt floods originated in the Rocky Mountain headwaters, had larger magnitudes, and carried coarser sand loads of lower concentration than floods that occurred later in the year (Webb et al., 1999; Topping et al., 2000a). Late summer floods originated in low-elevation tributaries by thunderstorms and were generally of smaller magnitude but carried more fine-grained sediment in suspension (Webb et al., 1999; Topping et al., 2000a). In the post-dam era, annual floods have been eliminated, and dam releases do not vary in the course of the year (figure 3).

Only in a few instances have dam releases been sufficiently large to approximate those of the pre-dam era. The highest of these and the only one similar in magnitude to the pre-dam annual average flood occurred in 1983, when discharge of the Colorado River in Grand Canyon reached 2750 $m^3/s$. Between 1984 and 1986, dam releases annually created peak discharges between 1275 and 1700 $m^3/s$. In spring 1996, a well-publicized and closely monitored controlled flood of 1275 $m^3/s$ occurred.

The annual flood regime of the Colorado River and the pattern of sediment inflow from tributaries in the pre-dam era created a season of sediment accumulation and a season of sediment evacuation in Grand Canyon (Topping et al., 2000a, 2000b). The season of accumulation of sediment was the nine months from July to March, and the

season of sediment evacuation was the three months from April to June. The period of annual sediment storage in the post-dam era is limited to two months, typically July and August after input events from tributaries (Topping et al., 2000a).

***The fan-eddy complex***

Eddies form in the lee of constrictions and are typically caused by tributary debris fans (Schmidt, 1990). In eddies, the lower velocities of recirculating flow, which are usually 0.1 times that of main flow, provide a low-energy environment conducive to deposition and the subsequent storage of fine-grained sediment (Schmidt and Rubin, 1995). This stored sediment is mobilized during floods. Eddies occur within fan-eddy complexes. Each complex includes a reach made up of an area of ponded flow upstream from the fan, a constriction near the fan apex, an expansion downstream from the fan where eddies form, and a mid-channel or channel-margin gravel bar (figure 4). Schmidt and Rubin (1995) asserted that fan-eddy complexes are the fundamental geomorphic assemblages of rivers with abundant debris fans. Fan-eddy complexes in Grand Canyon persist in fixed locations for time periods in the range of hundreds to thousands of years, allowing for monitoring of changes in the size of eddy bars that occur there.

Sand deposits in eddies commonly display similar characteristics. These characteristics led Schmidt (1990) to propose a classification of these bars. Deposits that mantle the downstream part of the fan are called separation bars; this term was adopted because the separation of main flow from the bank occurs here. Deposits near the reattachment point at the downstream end of each eddy are called reattachment bars. Reattachment bars project upstream from the reattachment point beneath the entire recirculating eddy. The upstream end of separation bars and the downstream end of

reattachment bars are the highest topographic points of these features (Rubin et al., 1990; Schmidt and Graf, 1990). During deposition, downstream ends of reattachment bars aggrade to the water surface and can be used as evidence of the stage of formative discharge.

Some fine-grained deposits in Grand Canyon do not form in eddies. These deposits are found on the channel-margins where the main flow is downstream but relatively slow. Other deposits occur in the lee of small obstructions, such as boulders and bedrock outcrops. Some deposits are found in the lee of mid-channel gravel bars (Schmidt and Rubin, 1995). These deposits are all referred to as channel-margin deposits for the sake of brevity.

## MONITORING CONSIDERATIONS

Monitoring is the "measurement of environmental characteristics over an extended period of time to determine status or trends in some aspect of environmental quality" (Suter, 1993). In the case of new monitoring programs, such as is being implemented in the Grand Canyon, many years of data collection may be necessary in order to detect long-term trends, and the National Research Council (1999) stated that, "a program designed to detect long-term … changes [in the Grand Canyon] should not be expected to yield significant results in the first few years". One strategy to determine long-term trends from a few years of monitoring is to place a short-term data set for a limited number of monitoring sites within the context of historical data, and that is the approach used in this paper. In doing so, one must overcome difficulties interpreting

historical data, because these data were not all collected under the same measurement protocols as the modern monitoring program, and that is the case in the Grand Canyon.

Typically, monitoring by land, water, or wildlife management agencies has a purpose. Monitoring may be conducted in order to detect long-term environmental change or its ecological consequences. Monitoring may serve as an "early warning system" of impending irreversible ecological change. Monitoring also may help decision makers evaluate whether management practices are achieving desired goals. In the case of the Grand Canyon, the primary objective of monitoring is to determine how operations of Glen Canyon Dam are affecting the downstream Colorado River ecosystem. Thus, an effective monitoring program must be able to detect significant changes in the size of sand bars and be able to distinguish reach-scale changes from inherent system variability. Operations of the dam have changed in response to a Record of Decision arising from an environmental impact statement (U.S. Department of the Interior, 1995), and an adaptive management program is underway wherein reservoir releases are altered in order to change some downstream ecosystem attributes. Monitoring is the basis of determining whether these operational changes are effective.

***Methods used in monitoring***

Monitoring of sand bars in Grand Canyon has occurred at a variety of scales and with variable precision and accuracy. Some studies have been done using repeated topographic surveys at selected sites. These surveys have been used to track changes in the area and volume of fine-grained deposits at these sites (e. g., Hazel et al., 1997; Kaplinski et al., 1995). Other studies have attempted a less quantitative, yet more comprehensive, approach by compiling an inventory of sand bars used as camping

beaches in order to track large-scale changes (e. g., Kearsley et al., 1994; Kearsley and Quartaroli, 1997). Schmidt and Leschin (1995) showed the feasibility of creating historical digital maps in vector polygon format, of surficial deposits in three reaches of the Colorado River, using aerial photograph interpretation and field measurements. Schmidt et al. (1999) and Grams and Schmidt (1999) showed the usefulness of these data for detecting historical trends in sand bar behavior as well as the response of bars to a single flow event, such as the 1996 controlled flood. These mapping techniques yield data that are coarser in precision than those collected by ground-based surveys. Schmidt et al. (1999) compared their techniques to detailed topographic surveys in order to assess their reliability. This comparison showed that the reported areas of erosion or deposition exceeding 0.25 m agreed with patterns determined from topographic and bathymetric surveys of the same areas. The extent of spatial agreement was 70% of the compared area. Mapping data comprehensively include all sand bars within a reach and therefore can be used to gain a better understanding of reach average conditions than can data from a few sites measured in detail. The average response of all bars in a reach is of value because individual sites may not necessarily be representative of the reach average condition (Schmidt et al., 1999).

## DESCRIPTION OF THE REACH ANALYZED IN THIS PAPER

The reach analyzed in this study is 14 km long and begins approximately 24 km downstream from Glen Canyon Dam near Lees Ferry (RM -0.9) and extends to just downstream from Badger Creek Rapid (RM 8.0). The Paria River enters the channel near the upstream end of the reach (RM 0.9). This reach is the upstream end of Marble

Canyon and occurs immediately downstream from Glen Canyon (figure 1). Throughout its length, this reach is within the boundaries of Grand Canyon National Park. This reach coincides with GIS site 17 and the downstream part of site 2, as designated by the Grand Canyon Monitoring and Research Center (GCMRC).

This section of Marble Canyon was termed the Permian Section by Schmidt and Graf (1990). The channel is wide in this section of the river, and the average ratio of top width to mean depth is 11.7. The average water surface slope in this reach, as determined by photogrammetry, is 0.0009 at 141 $m^3/s$. Calculation of this water surface slope was done using line coverages of topography in GIS sites 2 and 17 supplied by the GCMRC. The topographic base for site 2 was generated from aerial photos taken in 1990 at 141 $m^3/s$, but the base for site 17 was generated from aerial photos taken in 1993 at 226 $m^3/s$. The slope calculation was done for lower discharge, so a correction was applied to the water surface elevations reported for site 17. Ground-based surveys have reported that the difference in stage between the two discharges is approximately 0.5 m (Kaplinski, personal communication). Accordingly, values for water surface elevations from GIS site 17 were decreased by 0.5 m. The water surface slope calculated is less than values for other sections of the Colorado River through Grand Canyon (Schmidt and Graf, 1990; Schmidt et al., 1999). Schmidt and Graf (1990) reported that there are 0.4 campsites per mile in this reach and stated that most campsites are separation bars.

We analyzed this reach because we anticipated that the style of change near Lees Ferry would be more erosional than the style of change measured by Schmidt et al. (1999) further downstream (figure 1). Schmidt et al. (1999) did not detect differences in the characteristics of eddy bars in those reaches, despite the fact that the reaches are

located upstream and downstream from the LCR, and Schmidt (1999) had summarized other data from the 1996 controlled flood that indicated less aggradation in reaches upstream from the LCR. Thus, we applied our methods in this study to the reach where post-dam erosion was anticipated to be greatest and where the aggradation caused by the 1996 controlled flood was expected to be least.

## METHODS OF DATA ACQUISITION, INTERPRETATION, AND ANALYSIS

This section describes in detail the methods of acquisition, interpretation, and analysis of aerial photograph data using a GIS for the purpose of monitoring reach-scale changes of eddy sand bars. The sequence of activities is illustrated in figure 5. We emphasize techniques used to transfer data from aerial photo overlays into spatially correct digital maps, and the subsequent analysis of these data using GIS software.

### ***Data acquisition methods:***

#### *1) Photogeologic mapping*

Data synthesis began with interpretation and mapping of aerial photos. Available aerial photographs for dates between 1935 and September 1996 were mapped (Table 1). The mapping process began with the interpretation of surficial deposits as they appear on these photos when viewed stereoscopically. Map units were distinguished according to two criteria: 1) deposit facies and 2) formative discharge. The main focus of mapping was delineation and sub-classifications of fine-grained deposits.

Facies interpretations represent our interpretation of the depositional processes and grain size characteristics of each deposit. It was relatively easy to distinguish coarse

material, such as gravel, from fine-grained deposits, such as sand, silt, and clay, based on color and texture. For example, coarse-grained alluvium such as gravel and cobbles observed in this reach appear rough in texture and have a range of colors. On the other hand, fine-grained deposits appear smooth and light in color (figure 4). Facies of the fine-grained deposits was often recognized from the shape, location, and extent of these deposits (figure 4). For example, reattachment bars were recognized by their distinct shape. Recognition of eddy deposits was not always an easy task, however. In some cases, much of the eddy was filled by sand, and separation and reattachment bars merged. This made the distinction between the two bar types impossible. In these cases, these deposits were mapped as undifferentiated eddy deposits if they were located in the lee of a constriction such as a debris fan, or if the same deposit in other years exhibited obvious separation or reattachment bar form. The most important distinction to be drawn from mapping was distinguishing eddy deposits from channel-margin deposits.

Formative discharges were inferred from relative topographic elevations of flat-lying surfaces such as terraces. Each relatively flat-lying, terrace-like surface is inundated by a different discharge. We assumed that the discharge that inundated the deposit was also the discharge that formed the deposit. Relative elevation of each deposit was determined stereoscopically. Contacts were drawn at steep breaks in slope or where the color and texture of the deposit changed. Mapped formative discharge units in the study reach were divided into three categories: 1) the pre-dam high-elevation deposits that have not been inundated since closure of the dam, 2) post-dam flood deposits, which have only been inundated a few times, and 3) fluctuating flow deposits that are inundated daily. Category 2 deposits were further subdivided between those of the flood of 1983

and those deposited between 1984 and 1986. A complete list of facies and formative discharge characteristics of each map unit is described in Appendix A.

*2) Field Work*

Maps were field checked, and contacts were confirmed or corrected. Sedimentological description of some exposures was also conducted in order to determine flow direction during deposition; this was inferred from the migration direction of climbing ripples. Samples of fine sediment were also collected and sieved. These data were used in map unit descriptions (Appendix A). Stratigraphic relationships among deposits were also described. This activity allowed the distinction of mainstem flood deposits from tributary flood deposits. The differentiation was based on differences in sediment sorting, color, and interpretation of sedimentary structures.

***Integration of data into a GIS:***

*1) Digitizing the data and refinement to techniques*

The photogeologic data were mapped onto mylar overlays and then digitized using a more efficient technique than previously used. Schmidt and Leschin (1995) used a multi-step technique involving a stereo-zoom-transferscope to transfer overlay data of different scales onto a larger orthophoto-base at a scale of 1:2400. The process corrected for distortion inherent in aerial photos; it also allowed the mapping to be registered into a real-world coordinate system. However, this was a labor-intensive process, and allowed multiple opportunities for the introduction of human error.

For this study, the process of digitizing was modified by using ground control points along the river corridor to register each individual photo. This allowed the

mapping to be digitized directly from the mylar overlays of aerial photos, and eliminated the need for a stereo-zoom-transferscope; however, it necessitated the acquisition of real-world coordinates for ground control points. We examined the photos and identified permanent features such as large boulders and bedrock outcrops. These ground control points had to be visible in all photo-series. We selected a minimum of four control points for each individual photo in most cases. Figure 6 shows an example of a section of the river corridor as seen in an aerial photo and the ground control points used to register it. The real-world coordinates for the control points were obtained from orthophotos.

Orthophotos are compilations of a series of aerial photos planimetrically adjusted to accurate real-world coordinates such that all distortions inherent to aerial photos are corrected. In order to relate real-world coordinates to ground control points, each orthophoto sheet was registered onto the digitizing tablet, using points on the sheet with known real-world coordinates. Then ground control points were entered using the digitizing puck, each with a unique identification number and automatically registered real-world coordinates. The coordinates were recorded into a single file spanning the entire reach, and were incorporated into coverages to be digitized for each year of mapping.

The file used to store ground control points was identical in all coverages of mapping from all years of photography. During digitizing sessions, each photo was registered using identification numbers of the ground control points. In the case of some of the photos, more than four ground control points existed per photo but not all were visible due to scale or quality of photos; therefore not all control points were used.

However, more tics were used when possible in order to increase the spatial accuracy of the data set.

During digitizing sessions, root mean square (RMS) errors were often less than 3.0% for each registered photo. In cases when this number was exceeded, ground control points were re-entered and the photo was registered again if possible, in order to obtain a lesser error. In the case of some photos from the 1984 series, this was not possible due to the scarcity of ground control points, and the fact that the points were near the edges of the photos away from the nadir where distortion is greatest. Therefore RMS errors larger than 3.0% were accepted and coverages were later checked against coverages from other years of photography and digital orthophotos by overlaying them in Arcview and manually correcting overlay errors. Coordinates for the ground control points were obtained from projected orthophotos; therefore, GIS coverages did not have to be projected. They are in the State Plane Coordinate System zone 3176, with units in meters, and using the North American Datum of 1983, in accordance with data standards required by GCMRC.

*2) Constructing a longitudinal profile in order to check map units*

A longitudinal profile was constructed for the elevation of the water surface at each formative discharge associated with the map units (figure 7A). Elevations were determined for these deposits known to aggrade to near the water surface. The longitudinal continuity of map units for each formative discharge was then checked and unit designations were adjusted accordingly. If a surface thought to be associated with a given formative discharge was drastically higher or lower than the profile of other surfaces associated with the same discharge, it was assumed to have been misinterpreted

and mislabeled. All such anomalous units were checked and corrected. Figure 7B shows a final version of the longitudinal profile for the reach, after all corrections were made.

The data for the longitudinal profile were generated by overlaying the line coverages of topographic contours of GCMRC designated sites 2 and 17 on coverages from mapping from this study. A third line coverage of channel centerline was "screen-digitized" and overlaid in order to measure stream-wise distance.

*3) Comparison to studies on the Colorado River using similar spatial data*

Since the technique for transferring spatial data from original aerial photos differed from the method used by Schmidt et al. (1999), these differences were evaluated. This was not a test of accuracy in the strictest sense. It was a test of compatibility of the methods, in order to justify comparisons of our data with data from Schmidt et al. (1999). Leschin's original mylar overlays (unpublished) of a few photographs from October 21,1984, and June 2, 1990, were digitized using our method of planimetric adjustment. We compared these data with Leschin's unpublished coverages constructed using a stereo-zoom-transferscope. The comparison was done by onscreen measuring of the distance between the apparent shift in location of the same point, from the coverage created by the labor intensive method using a stereo-zoom-transferscope to the coverage created by our new direct-digitizing method. This allowed the quantification of the positional differences between the old and new method of digitizing. This method of analysis was similar to that used by Barrette et al. (2000). Seventy-eight points were compared in order to assess the difference between the 2 digitizing techniques. The deviation between the methods was less than 4 m in the x-y plane for 91.0% of the points. The maximum deviation of any point was 6.5 m (figure 8A).

*4) Accuracy in reporting locations*

As a more rigorous test of our digitizing method, locations of points on the digital maps were compared relative to corresponding locations on the digital orthophotos. We assumed that the orthophotos are the truth, meaning they report location with 100% accuracy. We used the same approach as described above to assess the accuracy of mapping done for this study in relation to digital orthophotos. Distances between points identified on orthophotos and those on coverages digitized directly from aerial photos were measured onscreen. We used the coverage from the 1990 photo series because this was the photo series used to generate the orthophotos for GIS reach 2. The aerial photos used for generating the orthophotos for GIS reach 17 were from 1993 (the only date orthophotos are available for this reach); for this comparison we used the coverage generated from 1990 mapping.

The independent test for the accuracy of the new method was performed using 58 individual measurements. Of these, 97% were within 4 m of the actual location, as shown on the orthophotos. Points within a 3-m radius of the actual location comprised 90% of the total. The maximum deviation from the actual location for the new method was 5.7m (figure 8B).

There are two possible sources of error in reporting location: 1) random error caused by human errors in mapping, the thickness of the pencil lines drawn, or inaccuracies in tracing the lines during digitizing due to errors in placement of the puck crosshairs; 2) systematic error due to distortions inherent to aerial photographs. The above analysis demonstrates the result of the combination of both of these types of error

in our data set. We quantified the portion of these errors associated with the method used to digitize our mapping. Most of the mapping for this project was done using a mechanical pencil with 0.3 mm lead thickness. This represents a line 1.4 m thick on the coverages created from the 1990 photo series, which are at a scale of 1:4,800. In order to quantify the portion of error due the digitizing process, we digitized into two separate GIS coverages, random scenes from mapping done from March 24, 1996. Distances were measured between corresponding points on the two coverages that represent the same location in the horizontal plane. Figure 8C is a histogram that represents the distribution of distances between locations reported in each coverage. Eighty-five measurements were made. The maximum deviation between two points representing the same location was 1.52 m (roughly equivalent to the thickness of the 0.3-mm pencil line on the aerial photo), and 69 of the points measured (81%) were within 1 m of their true location. This means that roughly 50% of the error associated with reporting locations in this data set is random error due to the method used to map and digitize aerial photos at this scale, and not due to systematic error inherent in aerial photos. Error associated with photos of 1935 would be the greatest in the data set, at approximately up to 9 m, because the photos from this time are the smallest in scale (approximately 1:30,000).

*5) Accuracy in reporting polygon area*

The most important aspect of the digital spatial data used for this study is their ability to report areas of polygons accurately. Quantification of the accuracy in reporting location is important, but it does not address the issue of how accurate the reported polygon areas are. The two factors that affect the ability to report locations described

above, also affect the ability to report areas of polygons in a data set. The most effective way to assess the overall accuracy in reporting polygon areas is to account for random errors as a result of the digitizing method and the systematic error as a result of distortion in aerial photographs, separately.

*A) Magnitude of random error due to scale of aerial photos and digitizing technique*

In order to quantify the errors in reporting areas associated with the digitizing technique, we digitized two random scenes from mapping done on photos of March 24, 1996 into two separate GIS coverages. Figure 9 shows the size distribution of the polygons generated, as averaged between the two coverages, demonstrating the range of sizes used in our analyses. We compared the areas of corresponding polygons and quantified the differences. These differences represent the possible range of errors associated with the method of digitizing. Figure 10A shows the absolute differences in area, and Figure 10B shows these values as percentages of areas of polygons compared. There is no correlation between the absolute difference in area and percent difference in area (figure 10C); polygons with the largest absolute error did not have the largest percent error. However, there is positive correlation between the sizes of polygons and the associated absolute magnitudes of possible errors in reporting area (figure 11A). There is an inverse correlation between the areas of polygons and percent error in reporting area (figure 11B). For the polygons tested, those larger than 1000 $m^2$ had less than 5% error associated with their reported areas; polygons larger than 300 $m^2$ had less than 7% error associated with their reported areas (figure 11B). This means that assuming there is no distortion in the aerial photographs, reported areas for polygons

larger than 300 $m^2$ are accurate to within $\pm$ 7%, and reported areas for polygons larger than 1000 $m^2$ are accurate to within $\pm$ 5%. This also indicates that the larger a polygon, the larger is the magnitude of possible error in reporting area; however, the area in error represents a smaller portion of the total area of the polygon. This disparity is the result of the fact that the magnitude of area of error is a function of the perimeter of the polygon and not the area; because deviations from the "true" line defining the boundary of the polygon are the cause of the error. The relationship between polygon areas and polygon perimeters in this data set is not a linear one (figure 12); increases in the areas of polygons are associated with smaller magnitudes of increase in the perimeter. There is positive correlation between the absolute magnitude of errors in area and polygon perimeters, and this correlation is a stronger one than that between absolute magnitude of errors and polygon areas (Figure 13A). There is an inverse correlation between the percent errors in area and polygon perimeters (figure 13B). This correlation is similar to the correlation between percent errors in area and polygon areas.

*B) Magnitude of systematic error due to distortion inherent in aerial photographs*

The systematic errors due to distortion in aerial photos are more difficult to quantify than random errors, because there is no way to compare areas of distorted polygons to areas of undistorted polygons. Furthermore, there is no way to quantify all errors in all aerial photographs used in this study. As a result we relied on approximations of the maximum range of this type of error. In order to approximate these errors we used the coverage containing the MPAEB's (introduced below) for simplicity; this coverage encompasses the entire length of the reach and has fewer

polygons. Nearly all polygons in this coverage are longer than they are wide. Lengths and widths of all the polygons in the coverage were measured and an average ratio between these dimensions was calculated; this relationship is of 1:5. For area approximations it was assumed that the "average shape" of the polygons in this data set is an ellipse. For the average polygon, there is a range of possibilities in reporting locations for different parts of the polygon, depending on its size and its location relative to the nadir of the photograph on which it was mapped. Figure 14A shows the extreme scenario of a given positional error with zero error in reporting area; this is the consequence of uniform positional shift (translation) from the actual location without distortion in scale. Figure 14B shows the opposite extreme scenario of a given positional error with the maximum possible error in reporting area for the polygon; this is the consequence of non-uniform positional shift from the actual location causing a distortion in scale as well as position. Both these cases are very unlikely; the actual range of error is most likely somewhere in between. Further, given the size range of polygons in this data set, the second scenario is even more unlikely; few polygons are large enough to encompass an area far enough apart and on opposite sides of the nadir to have been subject to this degree of distortion. Thus, we used the maximum possible error to define an improbable but possible extreme limit to the error in our data set. We used the "average" shaped polygon to describe all the polygons in the data set. The area of an ellipse as:

$$A = \pi Rr$$

where R is the major radius of the ellipse, r is the minor radius of the ellipse and $\pi = 3.14$. The percent error in reporting area therefore, can be reported as:

$$E = [ ( R + e ) ( r + e ) - Rr ] / Rr$$

where E is the percent error in reporting the area of the polygon, and e is the maximum linear distance from actual position of a point (i.e. maximum linear error describe above). Figure 15 shows the log-log relationship between percent error and area of the polygon as applied to this data set. As with random errors an inverse relationship exists between polygon area and percent maximum possible systematic error.

Overall error is reduced with increasing polygon size. We illustrated above that this is primarily because the magnitudes of error are more closely associated with polygon perimeters than with polygon areas, and that polygon perimeters (at least in this data set) do not have a direct relationship with polygon areas. It follows that given a constant polygon perimeter, a two-fold increase in errors associated with reporting location would cause a two-fold increase in errors associated with reporting polygon areas. This is the approximate relationship between the magnitudes of measured random errors and the magnitudes of measured overall error in reporting locations (figure 8B and C). Errors of up to 2 m in reporting location cause errors of less than 7% in reporting areas for polygons larger than 300 $m^2$; therefore, errors of up to 4 m (for 97% of points measured) would cause errors of no more than 14% in reporting areas of these polygons. For our analyses we used MPAEB's larger than 1000 $m^2$. When calculating fill ratios (introduced below) individual polygons within the area of interest are sometimes smaller in size than 300 $m^2$; however, the combined sizes of several of these polygons adjacent to each other are larger than this magnitude. Therefore, using them is still valid within the error range of less than $\pm$ 15%.

It is crucial to realize the limitations of precision in reporting spatial data if these data are to be used effectively. Both vector and raster data were used in this study. All

coverages resulting from mapping of aerial photos were vector polygon coverages. Coverages of eddy complex boundaries and erosion/deposition maps (discussed below) are consequently in vector format as well. These vector coverages report locations to the nearest 0.001 m. However, it should be noted that although the software allows a user to zoom in to great apparent precision, this does not mean the locations were accurate to the same degree. During analyses, we preserved the original precision of the data through multiple steps, and reduced significant digits after the final step. All areas were reported to the nearest meter, and all ratio data were reported to two significant figures. Raster grids were used only for assessing the reliability of the algorithm used to generate change maps. All grids were generated from the vector coverages, therefore, their positional accuracy was the same as the vector coverages.

***Analysis techniques and their accuracy:***

There are many strategies that can be used to analyze the GIS data described above. In this section, we describe how an objectively defined reference state can be calculated. Once this reference state is calculated, other metrics can be calculated which can be used to measure eddy bar conditions and changes through time. In this section, we describe how these metrics are calculated.

*1) The need for a reference state*

We must be able to compare the condition of each eddy sand bar to some standardized state in order to track changes in the reach. In the case of this study, such a reference state was needed for each eddy sand bar. The outline of an area encompassing

all the areas within the eddy, known to have been occupied by sand at some time on record, is one measure of the maximum potential extent for that sand bar. Schmidt et al. (1999) called this area a persistent eddy. This area was determined by overlaying coverages of all years of photography and lumping all areas occupied by sand in all of the photo-series used. This area is herein referred to as the "maximum potential area of the eddy bar" (MPAEB), which is a more descriptive term than "persistent eddy." MPAEB represents the largest contiguous area that has been occupied by sand in at least one of the available photo series analyzed in a reach (figure 16). The entire MPAEB was not occupied in its entirety by sand at any one time, however; different portions have been occupied by sand at different times. The MPAEB is also not the actual outline of the eddy; it defines the area where fine-grained deposits occur. There are some areas of eddies where no emergent or submerged sand was ever detected, therefore they are not included in the MPAEB. Thus, the MPAEB is an accounting concept that is objectively defined and allows us to compare the size of a sand bar from one time period to another relative to the objectively defined reference condition. This area can be expanded to include areas covered by sand in additional photo-series from other dates which may not have been included in these analyses.

The calculation of the MPAEB was done using **ARC/Info** software. An AML (ARC Macro Language) script was used to create a new coverage containing polygons that were the total area covered by sand in an eddy, in all photo years available. Lines separating polygons of the same eddy bar were removed to create a single polygon for each eddy complex. A modified version of the AML was created for application to the coverages of our study reach (Appendix B). The MPAEB's were assigned unique

identification numbers. In cases where there was no overlap between the separation and reattachment bars within the same eddy, distinct polygons were created automatically, and we manually assigned the same identification number to both polygons. Area of sand coverage within each MPAEB was determined for each year's mapping. The resulting coverages were used for the extraction of statistics for each eddy complex and to ultimately assess changes between the pre- and post-dam condition of sand bars in this reach.

*2) Determining areas of significant erosion and deposition between two consecutive photo series*

One of the most effective ways of quantifying the effects of a discrete flow event, such as the 1996 controlled flood, is to determine areas of significant deposition and erosion. Schmidt et al. (1999) did this by comparing coverages of pre-flood surficial geology to coverages of post-flood surficial geology, and tracking the changes in polygon classification. A simplified conceptual diagram of this process is shown in figure 17. Schmidt et al. (1999) used an AML script in **ARC/Info** to create maps depicting significant erosion and deposition in this way. We modified this AML to do the same for our coverages (Appendix C). First, two coverages were overlain. Then a new coverage with new polygons, subdivided by all the line features from both coverages, was created. These polygons retained all attributes from both input coverages. The new attribute field of "**change**" was added to the combined attribute tables of the polygon coverage. Those polygons with implied elevations, based on the map unit designation for formative discharge, that were less after the controlled flood than before the flood, were designated the attribute of "**erosion**" in the "**change**" field. Those polygons whose elevations were

higher after the flood than before, were designated the attribute of "**deposition**." Adjacent polygons with the same "**change**" attribute were then combined, eliminating the line features which defined their boundaries, and therefore generating a single larger polygon. What remained was a coverage containing larger polygons, with only the attributes of erosion, deposition, and no change (figure 17). The major assumption in using this algorithm was that discharge and therefore stage in both photo-series was equal.

*3) Determining the precision and accuracy of the areas of significant erosion and deposition*

The precision and accuracy of calculating areas of significant erosion and deposition for the 1996 controlled flood was determined by comparing our data with that of field surveys. Northern Arizona University (NAU) Sand Bar Studies Group has conducted detailed topographic and bathymetric surveys at two sites in the study reach for many years. These sites are at RM 2.3 and 8, upstream from Cathedral Wash and immediately downstream from Badger Creek Rapid, respectively. Raw survey data from pre- and post-flood 1996 were supplied by NAU. Data were imported as point data into **Arcview** and converted to floating point grids (figure 19A). Change grids were generated for each site by subtracting the elevation values of the post-flood grids from the pre-flood grids. All grids were generated with a 2.0 m cell size. These change grids were classified into areas of significant deposition, significant erosion, and no change, where significant change was determined to involve changes of 0.25 m or more in the vertical direction. Schmidt et al. (1999) had evaluated other thresholds of change that could be used to distinguish "significance" and found that the best agreement between survey and

map data was for 0.25 m threshold. In other words, if the elevation of a surface changed more than 0.25 m as a result of the controlled flood, it was considered to have experienced significant erosion or deposition. This is the same magnitude of change used by Schmidt et al. (1999). Coverages of change from photogeologic mapping for the areas in common with the detailed surveys were cropped onscreen and converted to grids (figure 19B). Change grids generated from photogeologic mapping were overlain on change grids generated from detailed surveys for comparison (figure 19C).

It became apparent that the AML for calculating areas of significant erosion and deposition used by Schmidt et al. (1999) was inappropriate for this reach. Field surveys in this reach indicate that part of AML used by Schmidt et al. (1999) overestimated the area of significant aggradation. In reaches studied by Schmidt et al. (1999), polygons that had been designated as "high flow sands of 1984-86" before the controlled flood and as deposits of the controlled flood afterwards had new deposition more than 0.25 m. Thus, the AML used by Schmidt et al. (1999) assigned the attribute of "deposition" to these change polygons. In our study reach, deposition was less than 0.25 m in these areas, and we modified our AML to assign the attribute of "**no change**" to these polygons.

We quantitatively compared our data with that derived from NAU field surveys and found good agreement. At the site at RM 2.3, 76% of the area compared was in total agreement between the two methods (table 2). This means that if we detected erosion or deposition in an area, the field surveys measured actual change of more than 0.25 m; and if we detected no change, the actual change was less than 0.25 m as measured by the field survey. At the site at RM 8, 68% of area compared was in total agreement. Of the

combined area of both sites, 72% was in total agreement (table 2). At the site at RM 2.3, 2.7% of the area compared was in total disagreement. Total disagreement occurred where our method reported erosion in an area where the topographic survey measured deposition, or vice versa. At the site at RM 8, 2% of the compared area was in total disagreement. Of the total compared area, 2.4% were in total disagreement.

In the remaining 25.6% of the compared area our method detected no change, and the field survey measured changes greater than 0.25 m, or vice versa. These areas make up 21% of the area being compared at RM 2.3, and 29.9% of the area at RM 8. The largest areas of this type of disagreement were areas of submerged sand, where field surveys measured erosion or deposition, but no change in elevation could be detected from photogeologic mapping.

It is important to keep in mind that the degree of agreement between the two methods did not involve any spatial corrections in the overlay of the two data sets. No "rubbersheeting" transformations were performed; therefore, disagreement between data sets may have been compounded by errors in reporting location by one or both of the methods. The ground based survey is probably more accurate, due to the proven accuracy of the method and the equipment available. Disagreements in reporting erosion, deposition, and no change reflect differences in reporting location as well as change detection.

*4) Metric describing bar size: Fill ratios*

The fill ratio is one essential metric of bar change. This ratio is the total area within each MPAEB that is occupied by subaerial sand, divided by the area of the MPAEB. Schmidt et al. (1999) first developed the fill ratio concept. To generate a fill

ratio for a specific eddy, coverages of each year's mapping were overlain with the coverage containing the MPAEB, and areas of sand coverage within each MPAEB were separated. This allowed the delineation of all polygons labeled as sand bars for each MPAEB, with that MPAEB's unique identification number. Data tables from the combined coverage containing polygon areas for each eddy were then exported from **Arcview** and analyzed in a spreadsheet program. Total areas of each sub-categories within each MPAEB were calculated. The resulting number was then divided by the total area of the MPAEB to produce a fill ratio for that particular level of fine sediment. Total area of sand within each MPAEB was also calculated for total fill ratio. The distribution of these ratios allowed the quantification of reach average eddy bar size, without bias according to size of MPAEB. Quantitative comparison of the distribution of fill ratio values from year to year for the reach yielded information about trends in the reach average size of eddy sand bars through time. Comparison of fill ratio values of different reaches for the same time period yielded information about longitudinal patterns in the behavior of sand bars along the river corridor.

*5) Adjustment of the eddy fill ratio to account for differences in discharge at the time of photography*

In order to construct a time series that allows comparison of sand bars in the reach at different times, we adjusted measured areas of sand bars to account for the fact that photos taken when the river is high will be biased to show smaller bars. Aerial photos mapped from different dates were at varying discharges (table 1) and it was necessary to make these adjustments. Schmidt et al. (1999) and Grams and Schmidt (1999) used topographic data from field surveys of detailed study sites to develop relationships

between exposed area and discharge, and used these relationships to adjust measured areas of sand bars to eliminate this bias. The topographic data used were collected at selected sites in each reach before and after the recession of the 1996 controlled flood. Thus, detailed data from field surveys are required to develop these relationships, and such data are not always available. Also, these detailed discharge vs. area relationships are known only for a handful of sites in the reach only for one date; the assumption that the same relationship holds for all other sites in an entire reach may be inappropriate.

We developed an alternate method by which adjustments could be made. We calculated the total area of sand in all MPAEB's mapped in each year of available aerial photos. The data points for all years were plotted and a best-fit power function curve was calculated to construct an area vs. discharge relationship for the entire study reach. (figure 20). This power function was used to calculate the proportional increase or decrease in measured bar area necessary so that data for all years could be compared for the normative condition of 141 $m^3/s$. The shape of the curve was used to approximate the general relationship between sand bar area and discharge. The exact x- and y-intercepts were assumed to be of little consequence. The proportional change applied to each year is summarized in table 3. We also calculated adjustment factors for downstream reaches analyzed by Schmidt et al. (1999) and compared our factors with factors they calculated (table 4). Our correction factors were less than 16% different form those of Schmidt et al. (1999) in all cases and less than 5% in many cases.

*6) Another metric describing bar size: area of flood deposits compared to potential area of deposition*

The MPAEB encompasses areas of high elevation sand deposited in the pre-dam era that have not been inundated since 1983, or even since 1963. In order to assess the effectiveness of a specific flood in eroding or depositing sand bars, only those parts of the MPAEB inundated by a specific flood should be used to calculate fill ratios. Thus, high-elevation areas above the maximum stage of a flood should not be included in the MPAEB. Thus, the evaluated area is the "maximum area of potential deposition" (Schmidt et al., 1999). In the case of the 1996 controlled flood, only those areas inundated by a discharge of 1275 $m^3/s$ were selected for each MPAEB, and used to calculate fill ratios. Comparing distributions of fill ratios for areas of potential deposition amongst reaches allows detection of longitudinal patterns in response to a flood event.

*7) Metrics describing change in eddy bar size due to a flood: net normalized aggradation*

The net style of change in specific eddies is determined by subtracting the total area of significant erosion from the area of significant deposition and normalizing this value by the MPAEB. For analysis of the effects of the controlled flood, a quantity termed net normalized aggradation (NNA) was used, defined as:

$$NNA = ( A_d - A_e ) / A_{mpaeb}$$

where $A_d$ = area of significant deposition in $m^2$, $A_e$ = area of significant erosion in $m^2$, and $A_{mpaeb}$ = area of MPAEB in $m^2$ (Schmidt et al., 1999). Comparison of the distribution of these values among the reaches allows detection of longitudinal patterns in the relative magnitude of significant deposition and erosion in response to a flood.

*8) Metric for evaluating how close the response of an individual site is to the reach average response*

One option for monitoring reach-scale trends in size of eddy bars is to select individual eddy bars most likely to be representative of the behavior of an entire reach. This allows more detailed analysis of fewer sites efficiently and quickly, and is based on knowing which sites behave in a "representative" way. For analyzing change in area of sand in each eddy compared to the average condition of the reach, the Z-score for each MPAEB was calculated as:

$$Z = | ( X_i - X_{ave} ) / s |$$

where $X_i$ = the fill ratio for a year of photography, $X_{ave}$ = the mean fill ratio of all eddies for that year, and s = the standard deviation for the mean fill ratio of eddy bars for each year of mapping (Grams and Schmidt, 1999). This value is calculated for each MPAEB for all years. The average Z-score for each eddy bar is the mean of the absolute values for all years of mapping. The absolute value is used to measure the magnitude of difference in both the positive and negative directions. The eddies with the lowest Z-scores are the ones with fill ratios closest to the reach average fill ratio, in all years of aerial photography analyzed; thus, they are the most representative sites within a reach, with respect to area.

*9) Statistical analyses*

Histograms of eddy fill ratio distributions and NNA were constructed for the study reach and these distributions were compared with distributions calculated for reaches downstream. The distributions of these data are nonparametric. Data sets also have different sample sizes due to lack of ability to map some eddy complexes in some

years of aerial photography. To insure the reliability of the statistical analyses, minimum sample size and minimum detectable difference were calculated. The minimum number of MPAEB's per year of mapping in order to detect differences greater than 10% with 90% accuracy with $\alpha = 0.05$, is 18. The number of MPAEB's in all data sets compared are greater than this value. In order to compare distributions of different data sets Mann-Whitney-U tests were used; this is the most commonly applied two-sample test for nonparametric data. All ties were included in comparisons, and 0.05% confidence levels were used for individual testing of each pair of data sets. Paired sample tests were performed on data sets for this reach at different points in time. The results of these tests were identical to the non-paired sample tests. In all cases the following hypotheses were tested:

$H_0$: the two sets being tested have equal distributions

$H_A$: the two sets being tested have unequal distributions

An issue often ignored in statistical testing of samples is the limits of reliability of tests because of sample size and confidence intervals. Many statistical tests are designed to compare distributions of data sets that are samples of populations by approximating the distributions of the populations. In most cases the data for this reach includes all eddy sand bars in the reach; this means the data sets are the population. The same is true for most data sets for the downstream reaches. When comparing the sand bars in the reach to themselves at different times, all differences are "real" as long as all MPAEB's are included. The statistical analyses in this study were conducted for comparisons involving cases when not all portions of the reach were mapped and when different reaches were being compared. The approach was to see if the data sets were from the "same river."

## DETECTION OF TEMPORAL AND SPATIAL TRENDS

The purpose of this section is to illustrate the application of the analytical techniques discussed above to the evaluation of historical changes of sand bars. This discussion is intended to represent the wide range of findings that arise from large-scale analysis of sand bars using aerial photograph data. We comprehensively discuss these findings in a later paper.

### ***Description of reach characteristics using a GIS***

Creation of comprehensive reach-length GIS coverages made it possible to describe the general geomorphic and hydrographic characteristics of the reach with more robust data. For example, we determined that the average channel width was approximately 110 m on March 24, 1996, at a discharge of 226 $m^3/s$. Average width was determined by dividing the water surface area in the reach by the reach length. This measure of width is much more robust than the data used by Schmidt and Graf (1990) to estimate channel width in the same reach. They used cross-sections measured at roughly 1.6-km intervals to estimate a width of 85 m (280 ft), measured at 847 $m^3/s$. Thus, their estimate is more than 20% narrower than the true width, despite the higher discharge at time of measurement.

The spatial data generated for a reach also allow determination of the number and size of eddies in the reach. These data are also critical to developing reach-scale sediment budgets. This reach has 37 eddies (figure 21A). Of the total, 31 of the MPAEB's are larger than 1000 $m^2$. There are 2.6 eddies per river kilometer, and 2.2

MPAEB's per river kilometer larger than 1000 $m^2$. This frequency of occurrence for eddies is less than in reaches mapped by Schmidt et al. (1999) downstream. Although the total number of eddies differs from reach to reach, distribution of the sizes of MPAEB's in this reach is similar to the distribution of MPAEB's in other reaches previously mapped by Schmidt et al. (1999) (figure 21B).

***Use of a simple metric to describe reach average change through time***

The average fill ratio of eddies in this reach has changed with time. Both raw and adjusted fill ratios from different time periods for this reach were computed in order to describe long-term trends of storage of fine-grained sediment in eddies. Those MPAEB's equal to or larger than 1000 $m^2$ were used for all comparisons in order to minimize potential errors; small mapping errors would appear as large changes in fill ratios in the smaller eddies. We analyzed raw and adjusted fill ratios because of the possibility that normalization of fill ratios could introduce errors to the data. Comparison of raw fill ratios show that the year when this reach had the least exposed sand was 1965 (figure 22A); this is the year with the highest discharge during time of photography (table 1). The year with the most exposed sand in the reach was 1935 even though discharge in the 1973 photo-series was the lowest of all photo-series mapped. There has been little change in raw fill ratios since 1984. Raw fill ratios in 1984 and in 1990 were similar, and were slightly higher than in 1996.

Comparisons of adjusted fill ratios showed very little variation in reach average fill ratios between 1951 and 1996 (figure 22B). The only statistically significant changes in fill ratio occurred between 1935 and 1951, and between 1973 and 1984. Fill ratios for

1935 were the highest of all photo series analyzed. Fill ratios for 1973 were the lowest of all photo series analyzed. We also compared the average fill ratios before and after dam closure. Fill ratios from all pre-dam years, and post-dam years including and following 1984 were combined, respectively. Years 1965 and 1973 were excluded, in order to exclude a possible period of adjustment. The two data sets (pre-dam vs. post-dam) were statistically different in their distributions; the pre-dam era had a higher distribution of fill ratios. Thus the reach average size of eddy bars was greater in the pre-dam era than during the period between 1984 and 1996, even though the changes from year to year were relatively small.

***Use of a simple metric to describe longitudinal trends over a long time***

Comparison of longitudinal differences in fill ratios for specific time periods permits the quantification of systematic longitudinal trends and also the effects of local reach geometry (figure 23). Comparisons with data of Schmidt et al. (1999) were made for time periods when discharges were equal in all reaches. Thus, we excluded the 1973 photo-series, when discharge was very different among reaches. Raw fill ratios were used in order to minimize potential errors introduced by adjustment of fill ratios, and because there is no need to adjust data when discharges are constant.

For these comparisons, we grouped the adjacent Tapeats Gorge and Big Bend reaches; we refer to the combined reach as the LCR reach. The Lees Ferry reach and the LCR reach displayed similar patterns of sand storage in eddies throughout the period of record, and this pattern was significantly different than that of the Point Hansbrough reach. Eddies in both the Lees Ferry and LCR reaches had more of their area occupied

by fine sediment than did the eddies in the Point Hansbrough reach in 1935. This is the only year when the median values of fill ratios in both the Lees Ferry reach and the LCR reach are significantly higher than the median value of fill ratios in the Point Hansbrough reach. Fill ratio distributions were similar among the reaches in 1965. This date was only two years after the closure of Glen Canyon Dam, during the first post-dam high flows and could represent a period of adjustment. Sometime between 1965 and 1984 the adjustment to the post-dam discharge and sediment transport regime was completed and a new pattern was established. By 1984, the Point Hansbrough reach had the highest fill ratio of all reaches. This pattern was consistent until April 1996; at this time the fill ratios for the Lees Ferry and LCR reaches were significantly lower than the fill ratios in the Point Hansbrough reach.

There were no statistically significant differences between the fill ratios of the Lees Ferry reach and the LCR reach in all years of mapping. Further, there were no statistically significant differences in fill ratios for years 1965 and 1990, among all reaches analyzed. In all other years, there were statistically significant differences in fill ratios between the Lees Ferry reach and the Point Hansbrough reach, or the LCR reach and the Point Hansbrough reach.

### ***Detection of longitudinal and temporal trends using categorized fill ratios***

We also evaluated longitudinal trends in fill ratios by partitioning the areas within MPAEB's into the three categories described above. We sought to determine if there were different trends in the response of relatively low elevation and high elevation sand deposits. Partitioning was possible for data from the years including and following 1984.

We used raw fill ratios for MPAEB's larger than 1000 $m^2$ for reasons discussed above. Fill ratios were plotted for our study reach for years 1984 to September 1996 (figure 24) in order to analyzed temporal patterns in reach average eddy bar size this reach. Fill ratios were plotted for all reaches for 1984 to April 1996 (figure 25) in order to analyze longitudinal patterns in reach average eddy bar size. Table 5 lists the results of statistical analyses used to test the data in figure 25.

High elevation deposits in this reach that were deposited by pre-dam floods and have not been inundated in the post-dam era, and are more extensive in this reach compared to downstream reaches and have changed little (figure 25A). This is also true of the pre-dam deposits in the Point Hansbrough reach. However, pre-dam deposits make up a much smaller proportion of fine-grained deposits in the Point Hansbrough and LCR reaches (figure 25B, C). In the LCR reach, there was some erosion of these deposits by March 1996.

High elevation deposits that are topographically lower than pre-dam deposits have been inundated only during rare floods in the post-dam era. They made up roughly half of the deposits affected in the post-dam era in this reach (figure 24B). This proportion was about the same as in the LCR reach (figure 25F). However, in the Point Hansbrough reach, the post-dam high-elevation deposits made up a slightly higher proportion of the total deposits in the reach (figure 25E). The sizes of these deposits were largely unaffected between 1984 and March 1996, however, their sizes increased in all reaches as a result of the 1996 controlled flood (figure 25D, E, and F). In the Lees Ferry reach, these deposits were significantly eroded within 6 months after the controlled flood (figure

24B). No similar data were available for September 1996 in the Point Hansbrough and LCR reaches.

Low elevation deposits inundated daily by power plant flows also did not change between 1984 and March 1996 (figure 25G, H, and I). However, these deposits were eroded by the 1996 controlled flood. In our study reach, the extent of these deposits increased to sizes similar to that prior to the flood within 6 months after the controlled flood (figure 24C).

### ***Ability to detect longitudinal variation in style of change caused by a single flood***

Longitudinal variations in the magnitude of significant erosion and deposition of fine sediment in eddies in response to a specific flood can be detected by measuring areas of significant erosion and deposition. The histogram of NNA values for the study reach showed almost exactly the same number of eddies where net erosion occurred as where net deposition occurred. These values were calculated and compared for MPAEB sizes larger than 1000 $m^2$ and 5000 $m^2$; the distributions did not differ (figure 26A, B, and C). Distribution of NNA for this reach was not statistically different from the distributions in reaches further downstream. This was despite the fact that visual examination of these distributions seems to indicate less depositional response in this reach compared to downstream reaches (figure 27) and the fact that we had to modify the change detection algorithm, as described above.

We also evaluated the aerial extent of all significant erosion and deposition areas in an effort to determine if eddy bars are more dynamic downstream. Thus, we calculated total area of significant erosion and deposition in all eddies. Figure 28A

shows the total area of deposition and the total area of erosion per river kilometer, in all reaches as a result of the 1996 controlled flood. Figure 28B shows the total area of deposition and erosion per unit area of MPAEB in all reaches. The total area of deposition in eddies was slightly smaller than the total area of erosion in the Lees Ferry study reach, but in downstream reaches the total area of deposition exceeded the total area of erosion. The sum of areas of erosion and areas of deposition could be considered the total area of reworking. The total area reworked per unit length was the smallest in extent in the Lees Ferry reach and largest in the LCR reach. There was a trend of increased bar reworking due to the flood, in the downstream direction.

The fill ratio percentages for potential areas of deposition for eddies larger than 1000 $m^2$ were plotted as histograms for both April and September 1996 (figure 29). Comparison of the data from the two dates indicated that little change took place in the six months following the controlled flood. Comparison of the histogram from April 1996 to those from downstream reaches suggest that eddies in this reach were emptier after the flood than reaches downstream (figure10 in Schmidt et al., 1999).

***Use of Z-scores to determine which sites are most representative of the reach***

Z-score values were calculated for eddies larger than 1000 $m^2$ and are listed in table 6. The eddy sand bar in MPAEB number 33 was determined to have the lowest Z-score value and is therefore the site that is most representative of the reach average fill ratio for all years mapped. This site is located on river left approximately at RM 7. Eddy sand bars 10 (RM 2.6) and 37 (RM 8) are detailed survey sites monitored by the NAU Sand Bar Studies Group. These sites ranked eighth and sixteenth respectively in Z-scores and therefore are not the best sites to represent the reach average condition for this reach.

# SUMMARY AND CONCLUSIONS

The analytical techniques described and illustrated in this paper demonstrate the effectiveness of using aerial photograph interpretation and GIS as monitoring tools in a debris fan-affected river with numerous eddies, such as the Colorado River in Grand Canyon. We used techniques first developed by Schmidt et al. (1999) and Grams and Schmidt (1999) and altered some details in order to improve efficiency in the process of incorporation and analysis of the data. The metrics we used for the analysis were: (1) measurement of areas of sand in relation to the maximum potential area of eddy bar (MPAEB), expressed as a fill ratio, (2) eddy fill ratios in relation to the potential area of deposition during a specific flood, (3) corrected fill ratios that remove the bias associated with differences in stage caused by differences in discharge at time of photography, (4) categorized fill ratios for discrete topographic levels of eddy bars, (5) net normalized aggradation, and (6) average Z-scores. We illustrated the effectiveness of these metrics as applied to a reach of the Colorado River. We demonstrated that there is a wide range of variation in the size of sand bars in this reach at any specific point in time, similar to the range of variation documented by Schmidt et al. (1999) further downstream. This variation causes complications in the interpretation of topographic data measured at a few monitoring sites, because these sites may not be representative of changes elsewhere in the reach.

Despite the wide variation in bar size from site to site, we can detect some temporal and spatial trends in eddy bar characteristics at the reach scale, because our data

are comprehensive. Detection of these changes sometimes requires adjustment for the bias introduced by differences in discharge at the time of photography or the analysis of discrete areas of sand bars at different elevations.

Some trends in the responses of sand bars are so widespread that they are detectable in all reaches we analyzed, despite the variability at individual sites. The most prominent of these trends is the effect floods have on bar topography. We demonstrated that sand was eroded from the low elevation parts of eddy bars and deposited in the high elevation parts as a result of the 1996 controlled flood. Our analysis of eddy fill ratios for deposits at discrete elevations made the detection of this effect possible. We found that this effect no longer existed six months after the flood; high-elevation flood deposits eroded and the average size of low-elevation deposits increased. The average sizes of both categories of deposits were similar to their pre-flood magnitude in September 1996. Hazel at al. (1999) demonstrated this trend with precise ground surveys, and our findings demonstrate the widespread nature of this mode of geomorphic adjustment.

The ability to detect existing system-wide geomorphic trends suggests that the reason some other system-wide trends were not detected is because they do not exist. We hypothesized that extensive erosion of sand bars has taken place in the Lees Ferry reach compared to downstream reaches, as a result of changes to hydrologic and sediment transport regimes caused by the closure of Glen Canyon Dam. Our data do not support this hypothesis. We found that eddy bars in this reach behave more like eddy bars in the LCR reach and less like the eddy bars in the Point Hansbrough reach, despite the fact that the LCR reach is further downstream than the Point Hansbrough reach. The average size of eddy bars in the Point Hansbrough reach has been typically larger than the eddy bars in

the Lees Ferry and LCR reaches in the post-dam era. Thus, we found no evidence of a correlation between the average size of sand bars and proximity to the dam. The full historical analysis of these data is presented in a later paper.

The calculation of average Z-score values for identifying the most representative eddies in the reach suggests a strategy for identifying sites for long-term monitoring. Monitoring sites that display the most average geomorphic characteristics for the reach are the best candidates to be studied in detail.

Interpretation of aerial photographs and analysis within a GIS is not a complete substitute for detailed field measurements. Algorithms developed to detect change in bar topography must be calibrated by field measurements. Detailed field measurements of bar size, and changes in size, are critical inputs to a wide range of conceptual and numerical models. Nevertheless, the analysis of data derived from aerial photographs within a GIS allows objective determination of a reference state and calculation of the variance in bar behavior that is essential in interpreting system-wide changes in a complex system. The techniques of spatial analysis outlined in this paper are simple and basic, and for this reason promising in studying bedrock incised rivers.

Table 1- Aerial photograph information

| Date | Scale | Discharge in $m^3/s$ | Agency and Series |
|---|---|---|---|
| December 31,1935 | 1:30,000-1:35,000 | 85-170 | 3-282 to 3-284 |
| October 6, 1951 | 1:10,000[1] | 145 | GS-QZ 15-108 |
| September 25,1952 | 1:10,000[1] | 290 | SCS[2] 11-138 to 11-142 |
| October 8, 1952 | 1:10,000[1] | 180 | SCS GCES 20-52 to 20-55 |
| May 14,1965 | 1:12,000 | 730 | GCES[3] 0001- 0012 |
| June 16,1973 | 1:14,400 | 75 | GCES 0002-0022 |
| October 21, 1984 | 1:3,000 | 141 | GCES 1-115 to1-194 |
| June 2,1990 | 1:4,800 | 141 | GCES 11-1 to 13-17 |
| March 24, 1996 | 1:4,800 | 226 | GCES 11-1 to 13-17 |
| April 4, 1996 | 1:4,800 | 290 | GCES 11-1 to 13-17 |
| September 1, 1996 | 1:4,800 | 226 | GCES 11-1 to 13-17 |

[1] Enlarged from negatives
[2] Soil Conservation Survey
[3] Glen Canyon Environmental Studies

Note:
Discharges are estimated using detailed 15-minute-interval stage recordings from USGS gage 09382000, and release data from Glen Canyon Dam (Topping, personal communication). For photos without recorded time of day, the time of photography was estimated using lengths of shadows produced by canyon walls. A 3-hr travel time was assumed for water stage, from the dam to this reach.

Site at RM-2.3

Areas determined by topographic/bathymetric survey

| Areas Determined by photogeologic mapping | Erosion | No change | Deposition |
|---|---|---|---|
| Erosion | 1488 | 64 | 48 |
| No change | 340 | 380 | 120 |
| Deposition | 48 | 224 | 856 |

Site at RM-8.0

Areas determined by topographic/bathymetric survey

| Areas Determined by photogeologic mapping | Erosion | No change | Deposition |
|---|---|---|---|
| Erosion | 44 | 184 | 72 |
| No change | 148 | 2320 | 520 |
| Deposition | 8 | 304 | 260 |

Table 2- Areas in square meters of total agreement, total disagreement, and less severe disagreement, between our method of determining significant erosion and deposition, and that based on field surveys.

Table 3- Correction factors used to adjust fill ratios with respect to discharge in this reach.

| year | normalization factor |
|---|---|
| 1935 | 0.91 |
| 1951 | 1 |
| Sep-52 | 1.36 |
| Oct-52 | 1.1 |
| 1965 | 1.8 |
| 1973 | 0.68 |
| 1984 | 1 |
| 1990 | 1 |
| Mar-96 | 1.26 |
| Apr-96 | 1.37 |
| Sep-96 | 1.26 |

Table 4- Correction factors derived using the new method, and compared to those used by Grams and Schmidt (1999).

| | old method | new method | | | |
|---|---|---|---|---|---|
| year | average | TG | BB | average | % difference |
| 1935 | 0.87 | 0.76 | 0.88 | 0.82 | 5.75 |
| 1965 | 1.80 | 1.85 | 1.24 | 1.55 | 14.17 |
| 1973 | 1.12 | 1.18 | 1.05 | 1.12 | 0.45 |
| 1984 | 0.88 | 0.77 | 0.91 | 0.84 | 4.55 |
| 1990 | 0.71 | 0.73 | 0.91 | 0.82 | 15.49 |
| 1992 | 1.00 | 1.00 | 1.00 | 1.00 | 0.00 |
| 1993 | 1.00 | 1.00 | 1.00 | 1.00 | 0.00 |
| 1996.2 | 1.02 | 1.00 | 1.00 | 1.00 | 1.96 |
| 1996.3 | 1.02 | 1.24 | 1.13 | 1.19 | 16.18 |

Table 5- The results of statistical analyses of categorized fill ratios for this study reach and reaches downstream analyzed by Schmidt et al. (1999).
"R" denotes rejection of the null hypothesis, and "F" denotes failure to reject.
The null hypothesis states that distributions of any two data sets are equal.

| Topgraphic level | year | Lees Ferry to Pt. Hansbrough | Lees Ferry to LCR | Pt. Hansbrough to LCR |
|---|---|---|---|---|
| High pre-dam terrace | 84 | R | R | F |
| | 90 | F | F | F |
| | Mar-96 | R | R | R |
| | Apr-96 | R | R | R |
| Post-dam flood sand | 84 | R | F | R |
| | 90 | R | F | R |
| | Mar-96 | F | F | R |
| | Apr-96 | R | F | R |
| Powerplant level sand | 84 | F | F | R |
| | 90 | F | F | R |
| | Mar-96 | F | F | R |
| | Apr-96 | F | F | F |

Table 6- Average Z-score values for the Lees Ferry reach. Fill ratio data are adjusted with respect to discharge. "n" indicates the number of years each eddy bar was mapped. Ranks are in descending order for all ranked values except average Z-scores; these are ranked in ascending order. Eddy bars with the lowest average Z-score values are the most similar to the reach average condition. Highlighted rows indicate eddy bars at sites monitored by the NAU sand bar studies group.

| | | | | | | Ranks of values | | | |
|---|---|---|---|---|---|---|---|---|---|
| Persistent Eddy | Eddy Area (m2) | n | Mean Fill Ratio, 1935-96 | Standard Deviation of Fill Ratio, 1935-96 | Average Z-Score 1935-90 | Eddy Area | Mean Fill Ratio, 1935-96 | Standard Deviation of Fill Ratio, 1935-96 | Average Z-Score |
| 33 | 20861 | 9 | 0.52 | 0.16 | 0.25 | 2 | 14 | 20 | 1 |
| 19 | 14374 | 9 | 0.43 | 0.10 | 0.25 | 6 | 20 | 28 | 2 |
| 30 | 14943 | 9 | 0.53 | 0.15 | 0.26 | 5 | 13 | 23 | 3 |
| 36 | 15165 | 10 | 0.46 | 0.13 | 0.29 | 4 | 18 | 26 | 4 |
| 11 | 2528 | 10 | 0.47 | 0.14 | 0.30 | 24 | 17 | 24 | 5 |
| 2 | 3850 | 8 | 0.36 | 0.10 | 0.31 | 19 | 24 | 31 | 6 |
| 29 | 1956 | 10 | 0.38 | 0.17 | 0.37 | 27 | 21 | 18 | 7 |
| 10 | 11820 | 10 | 0.54 | 0.10 | 0.38 | 9 | 12 | 30 | 8 |
| 18 | 5852 | 10 | 0.50 | 0.16 | 0.42 | 16 | 16 | 21 | 9 |
| 4 | 66983 | 10 | 0.50 | 0.19 | 0.43 | 1 | 15 | 11 | 10 |
| 23 | 1934 | 9 | 0.55 | 0.17 | 0.46 | 28 | 11 | 17 | 11 |
| 27 | 2193 | 8 | 0.59 | 0.20 | 0.53 | 25 | 10 | 9 | 12 |
| 16 | 2988 | 7 | 0.65 | 0.10 | 0.54 | 22 | 7 | 29 | 13 |
| 26 | 2732 | 7 | 0.62 | 0.24 | 0.55 | 23 | 8 | 4 | 14 |
| 28 | 4512 | 10 | 0.61 | 0.14 | 0.59 | 18 | 9 | 25 | 15 |
| 37 | 16912 | 10 | 0.43 | 0.18 | 0.60 | 3 | 19 | 14 | 16 |
| 32 | 13841 | 10 | 0.69 | 0.20 | 0.61 | 8 | 4 | 10 | 17 |
| 17 | 5303 | 10 | 0.37 | 0.17 | 0.64 | 17 | 22 | 16 | 18 |
| 22 | 6653 | 9 | 0.33 | 0.17 | 0.65 | 15 | 25 | 19 | 19 |
| 24 | 1743 | 7 | 0.22 | 0.19 | 0.66 | 31 | 28 | 12 | 20 |
| 25 | 1891 | 10 | 0.67 | 0.13 | 0.70 | 29 | 5 | 27 | 21 |
| 34 | 6881 | 8 | 0.67 | 0.24 | 0.78 | 14 | 6 | 5 | 22 |
| 12 | 8761 | 10 | 0.29 | 0.17 | 0.83 | 11 | 26 | 15 | 23 |
| 20 | 1975 | 9 | 0.27 | 0.23 | 0.87 | 26 | 27 | 6 | 24 |
| 9 | 6977 | 10 | 0.73 | 0.19 | 0.98 | 13 | 3 | 13 | 25 |
| 5 | 13956 | 9 | 0.21 | 0.22 | 1.04 | 7 | 29 | 8 | 26 |
| 14 | 1839 | 10 | 0.36 | 0.22 | 1.11 | 30 | 23 | 7 | 27 |
| 15 | 3532 | 8 | 0.84 | 0.36 | 1.22 | 20 | 2 | 2 | 28 |
| 31 | 10520 | 10 | 0.18 | 0.15 | 1.29 | 10 | 30 | 22 | 29 |
| 13 | 3086 | 9 | 0.15 | 0.29 | 1.35 | 21 | 31 | 3 | 30 |
| 35 | 7869 | 10 | 0.89 | 0.39 | 1.44 | 12 | 1 | 1 | 31 |

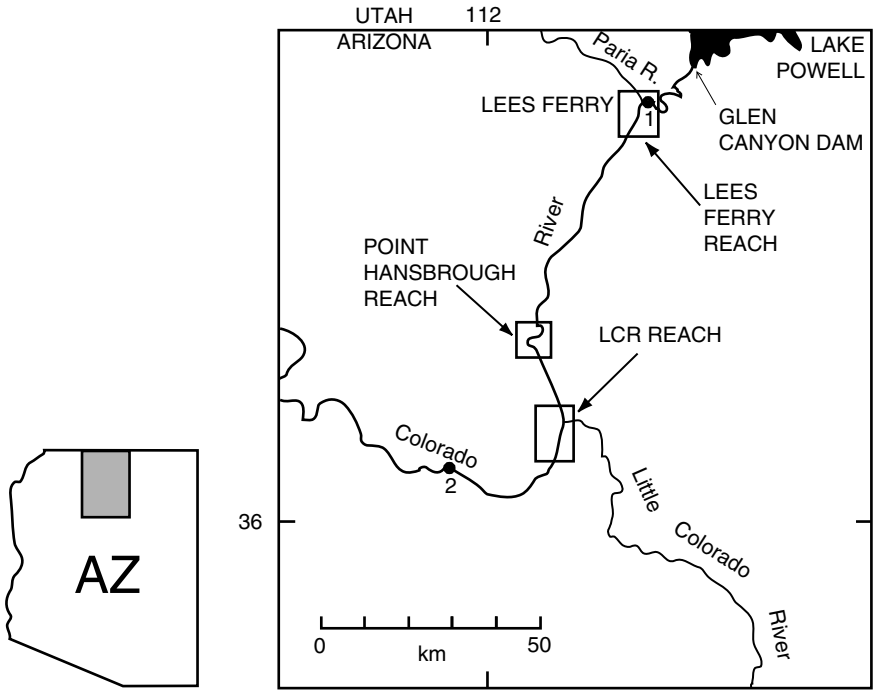


Figure 1- Site map of study reach. Point Hansbrough and LCR reaches are those analyzed by Schmidt et al (1999). The LCR reach is composed of the Tapeats Gorge and Big Bend reaches. (1) is USGS gage at Lees Ferry; (2) is USGS gage near Bright Angel Creek.

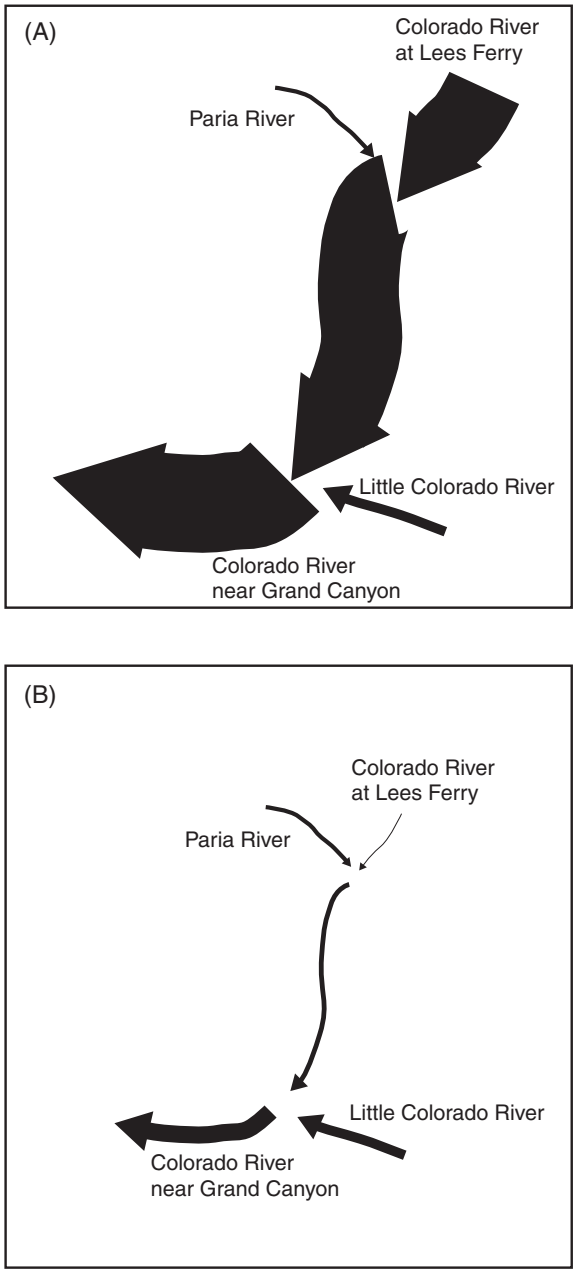


Figure 2- Pre-dam (A), and post-dam (B) concentrations of suspended sediment in the Colorado River. Relative line thicknesses indicate relative magnitude of concentration. Relationships were developed from data in Topping et al. (2000a).

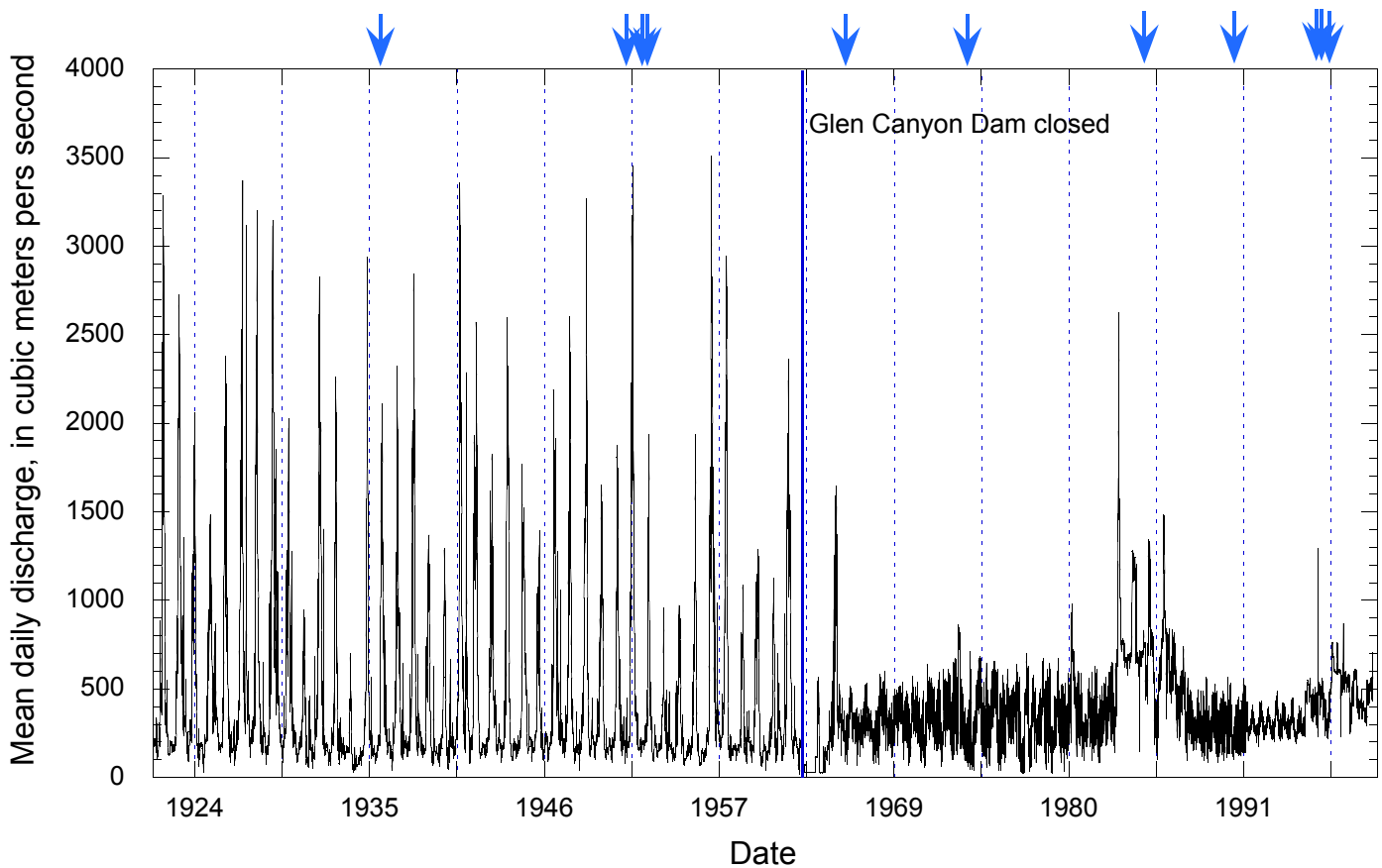


Figure 3- Mean daily discharge of the Colorado River at Lees Ferry (USGS gaging station 09250000) for years 1922-1999. Glen Canyon Dam was closed in spring 1963. Arrows indicate dates of aerial photographs analyzed in this study.

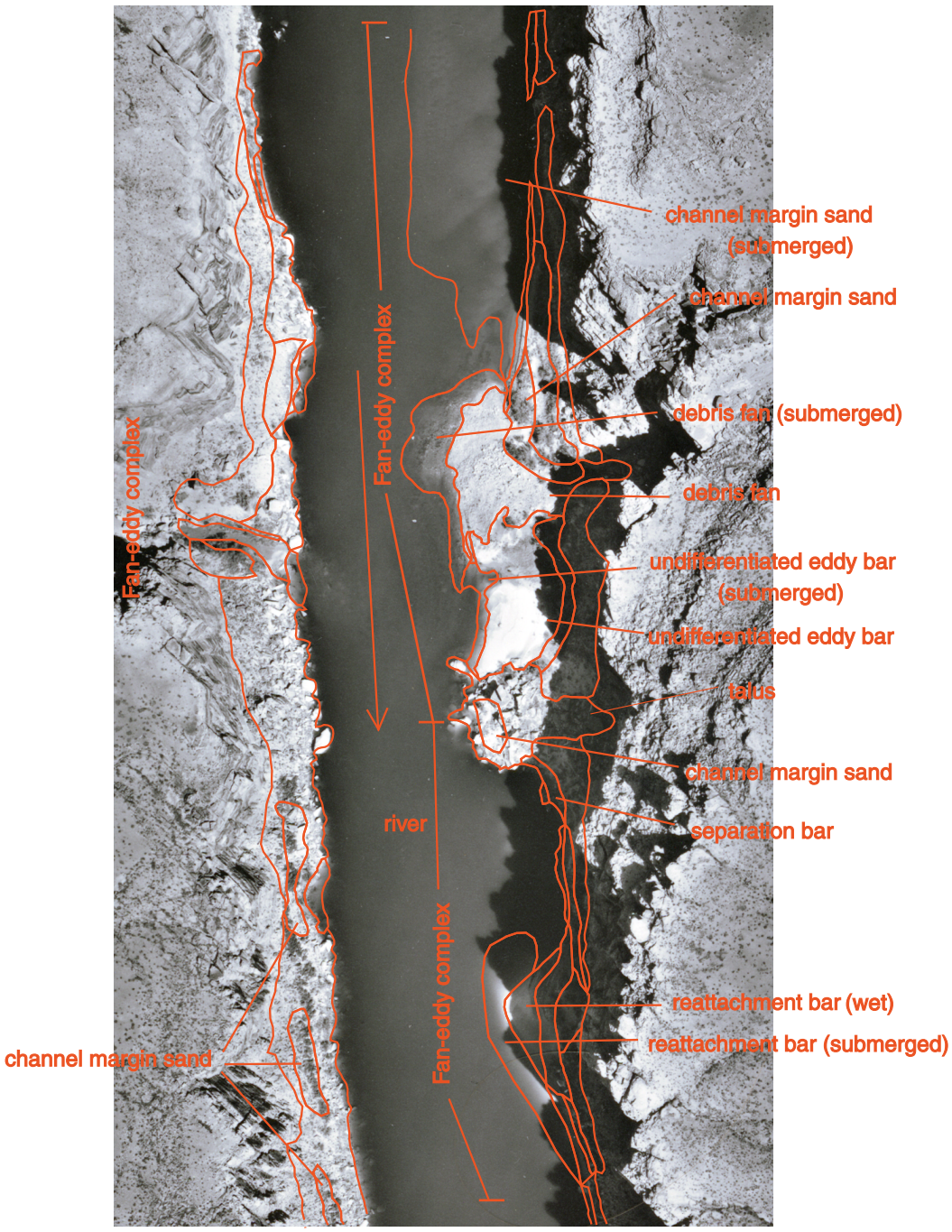


Figure 4- View of two fan-eddy complexes above Cathedral Wash as seen on aerial photos of April 4, 1996. Polygons of surficial geology map units are also shown. These units are described in the text. These fan-eddy complexes are closely spaced and there is no ponded area upstream from the downstream constriction. There are also no downstream gravel bars in either fan-eddy complex.

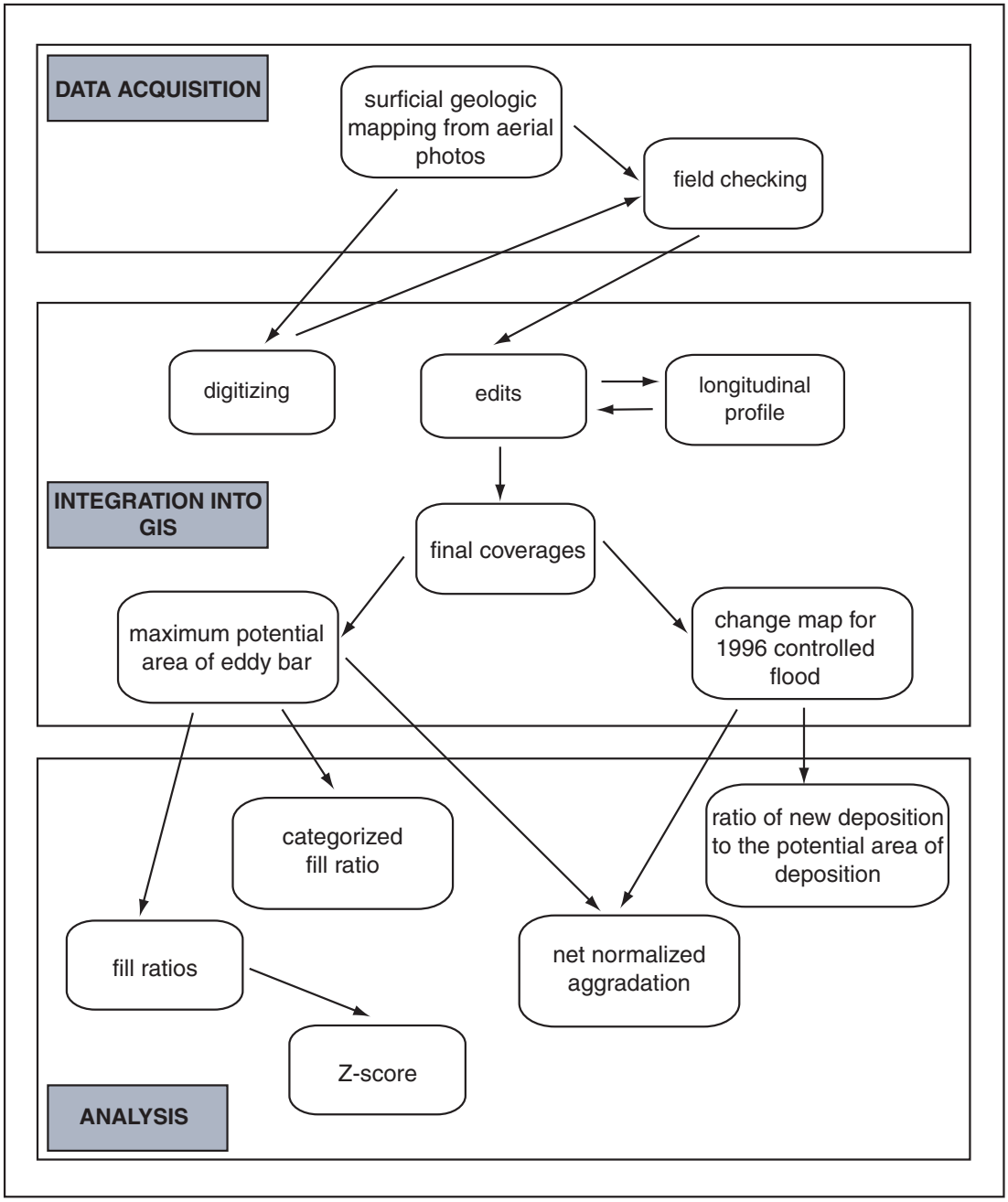


Figure 5- Conceptual flow chart of steps in data acquisition, integration into a GIS and analysis as used for this study.

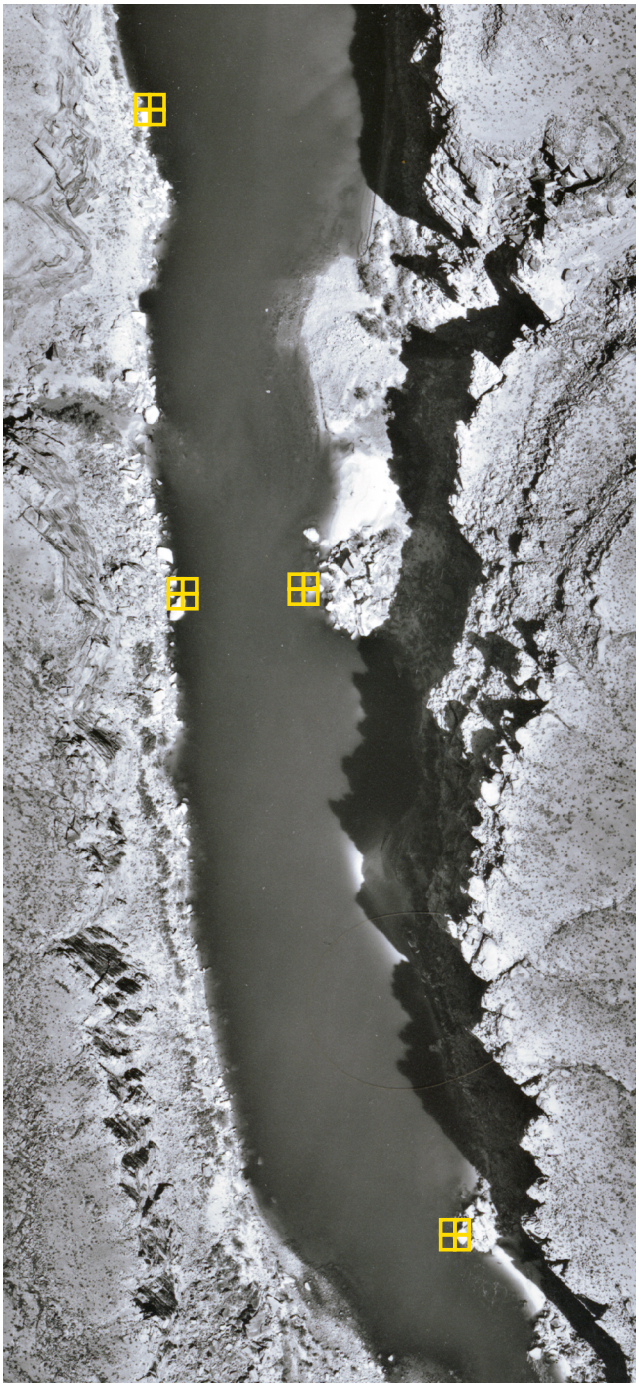

Figure 6- Aerial photo of the reach above Cathedral Wash on April 4, 1996. The yellow symbols are ground control points used to register the photo for digitizing.

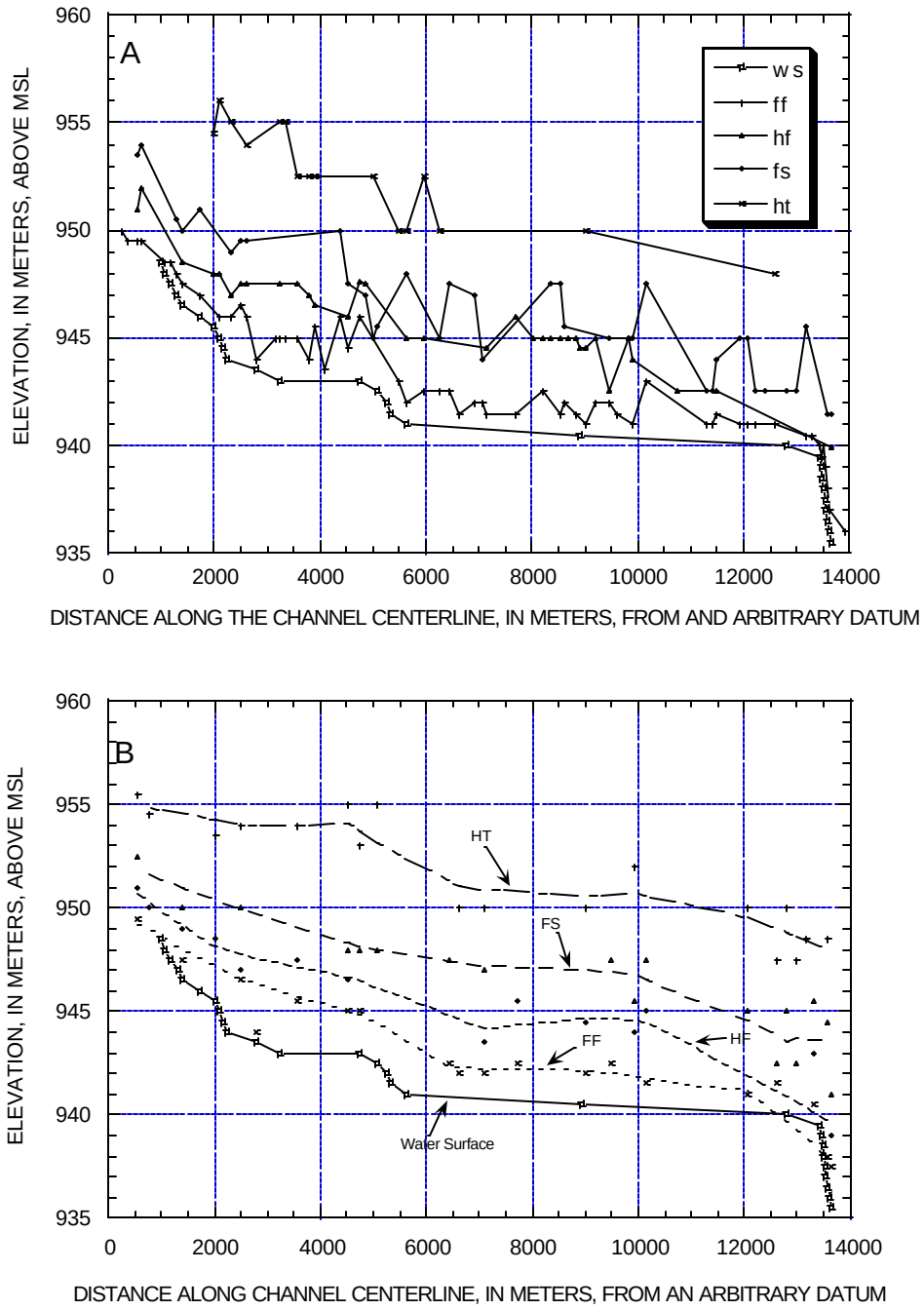


Figure 7- Longitudinal profile of water surface, power plant level sand (ff), high-flow level of 1984-86 (hf), 1983 flood stage level (fs), and pre-dam high terraces (ht), before edits (A), and after edits (B). Lines connect all points in (A). The lines in (B) are best fit lines using an automated smooth linear interpolation after misidentified points have been edited.

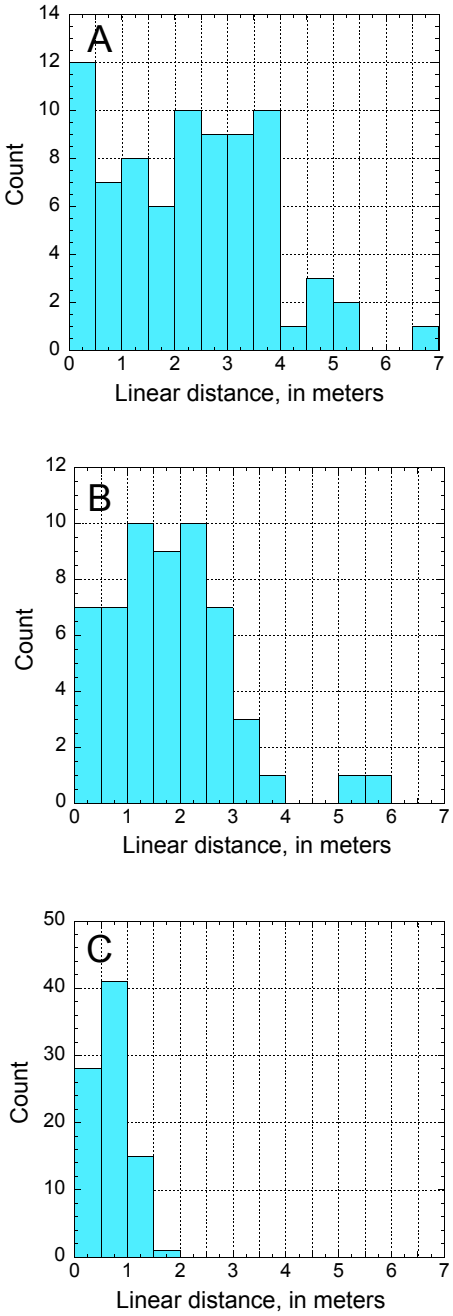


Figure 8- (A) Differences in positions reported between two methods of digitizing, one using a stereo-zoom-transferscope to scale mapping and the other directly digitizing each aerial photograph; (B) distance between locations reported on coverages and actual location as indicated by digital orthophotos, indicating total positional error in data set; (C) differences in position between separate sessions of digitizing the same scene, indicating random errors associated with digitizing method.

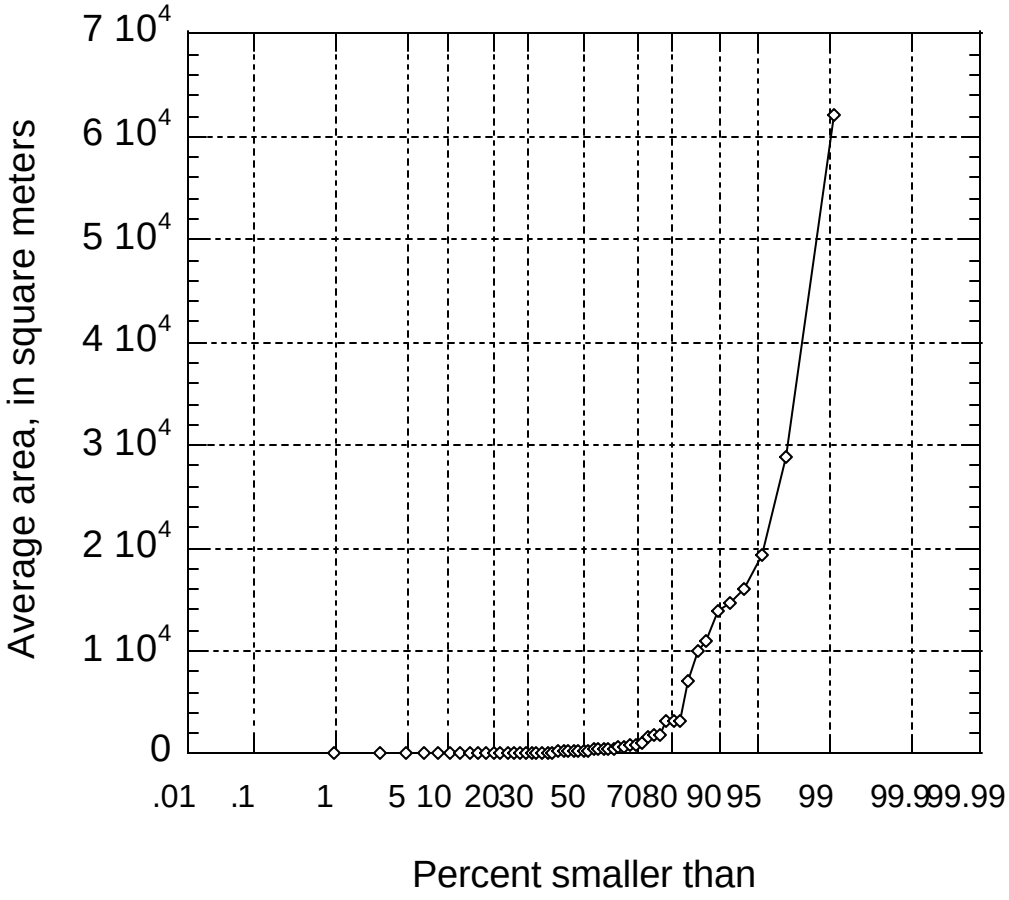


Figure 9- Distribution of polygon sizes averaged between two coverages, digitized to test range of variability in reporting location using the method of digitizing described in this study.

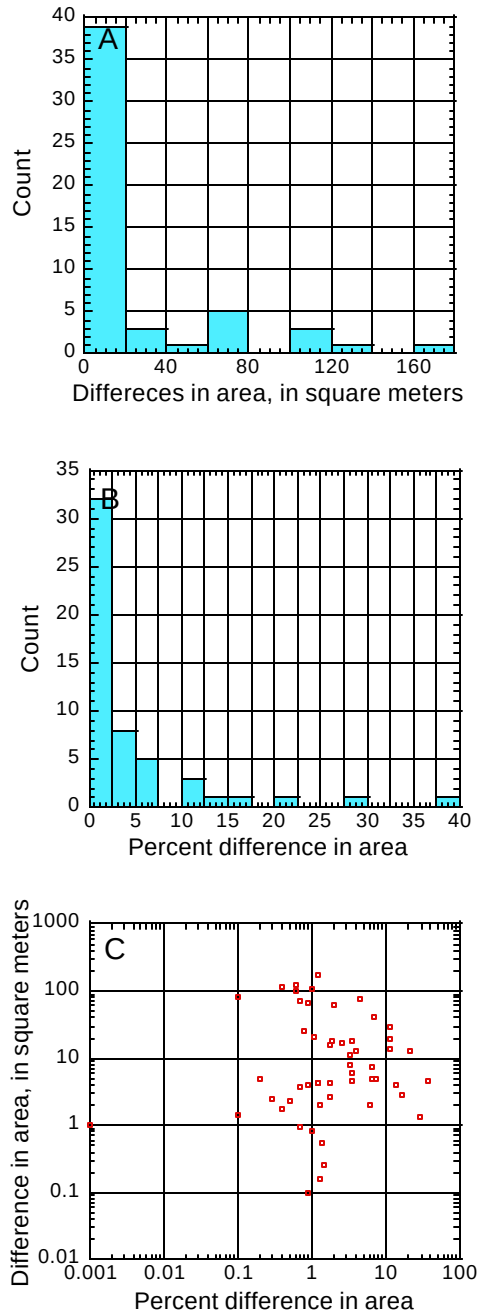


Figure 10- (A) Differences in linear distance for reported position in the horizontal direction, in square meters; between identical scenes digitized during separate digitizing sessions; (B) percent difference of polygon area for the same data set; (C) relationship between absolute differences in area and this value as percent ratio of polygons. Note: there is no correlation between the axes in (C)

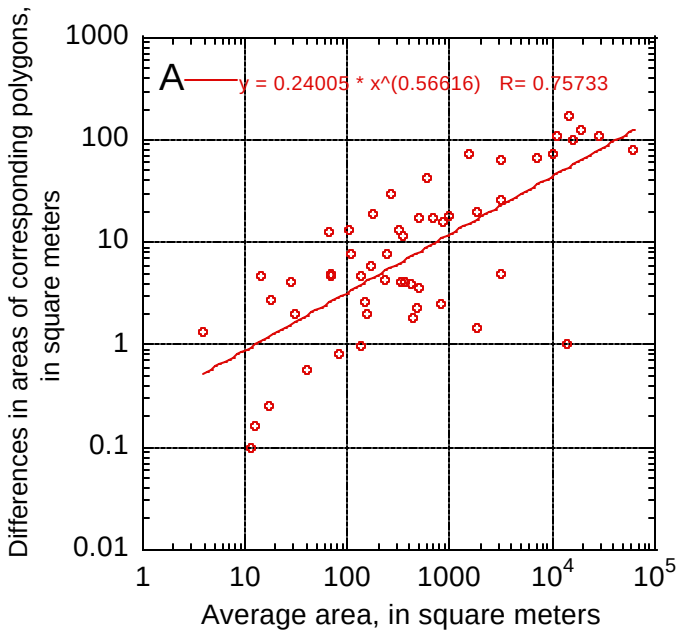


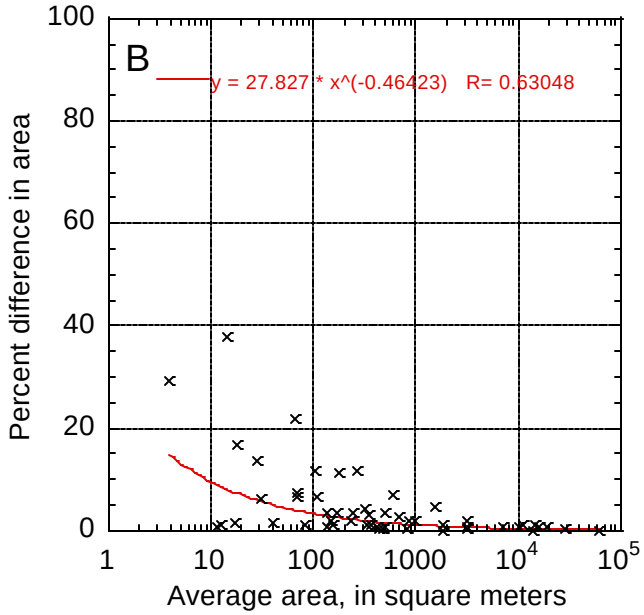


Figure 11- (A) Differences in areas of corresponding polygons from two separate coverages, compared to the area averaged between the two coverages; (B) percent differences in areas of corresponding polygons compared to the averaged polygon size. Note the R-values for both plots.

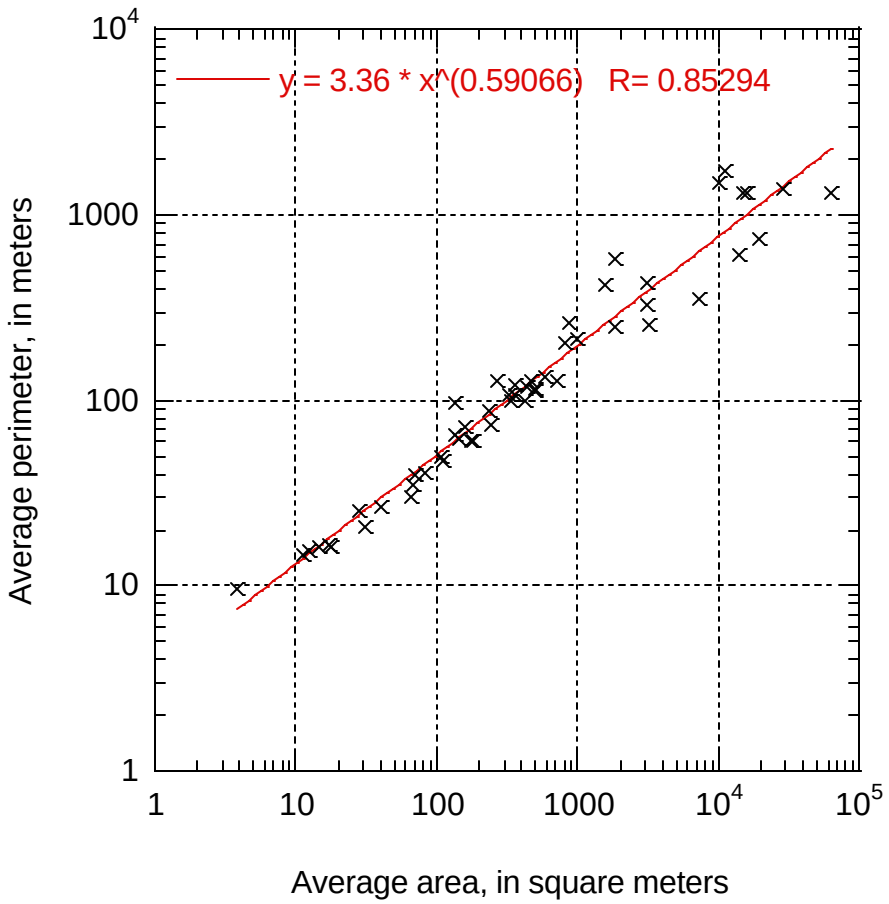


Figure 12- Relationship between areas of polygons and their perimeters, for the coverages digitized to test the spatial accuracy of the digitizing method used in this study. The R-value is that for a relationship described by a power function.

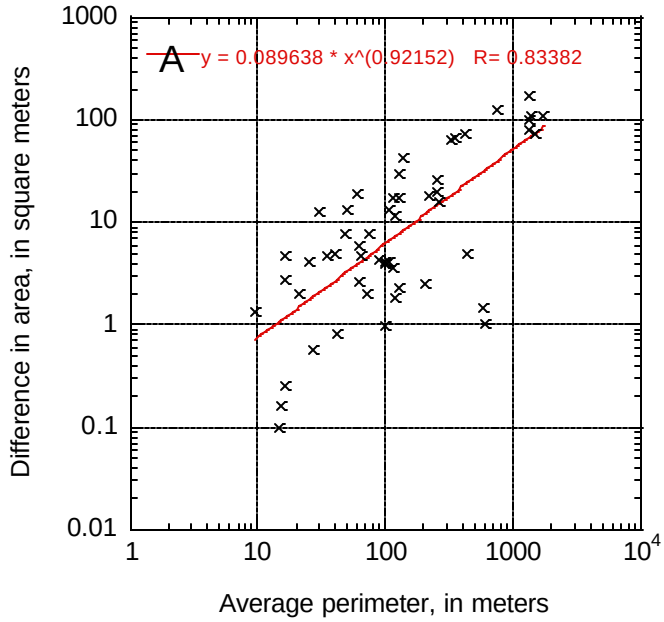


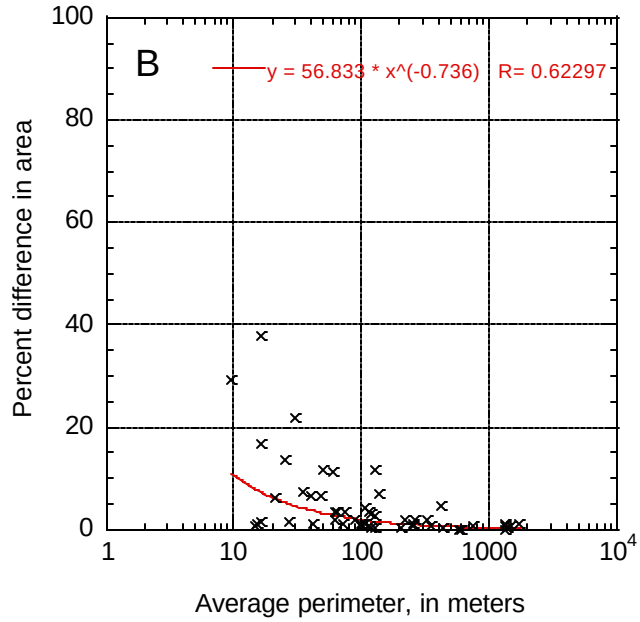


Figure 13- (A) Differences in areas of corresponding polygons from two separate coverages, compared to the perimeter averaged between the two coverages; (B) percent differences in areas of corresponding polygons compared to the averaged polygon perimeter. Note the R-values for both plots.

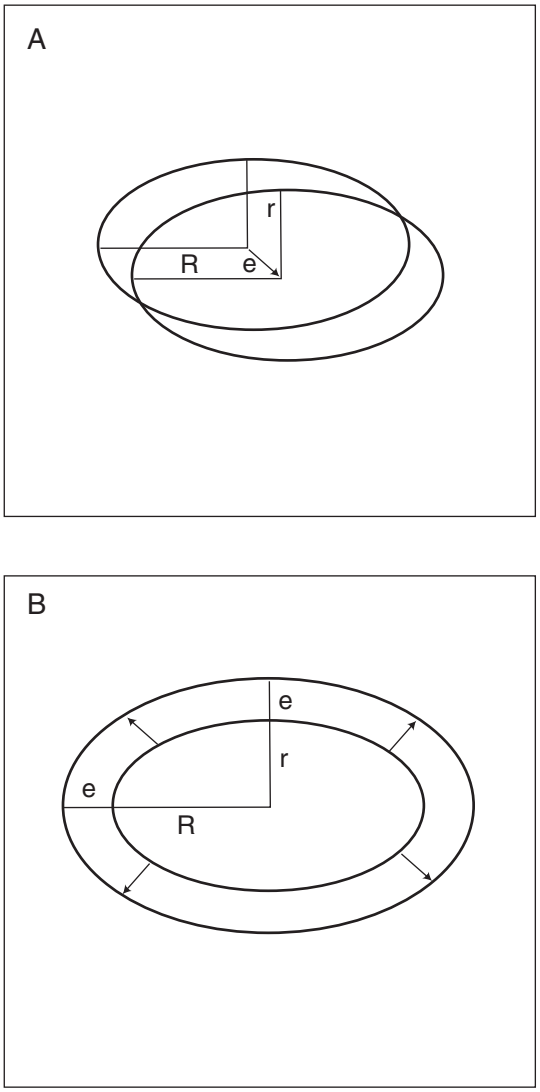


Figure 14- Scenarios for describing systematic error due to distortion in aerial photographs, (A) with maximum error in reporting location but no error in reporting area, due to uniform shift for the entire polygon (translation); (B) with maximum error in reporting location and maximum error in reporting area, due to non-uniform shift from one end of the polygon to the other end. Both these scenarios are unlikely, although (B) is more unlikely, because few polygons in the data set are large enough to have been far enough on opposing sides of the nadir during mapping to have been shifted in opposite directions.

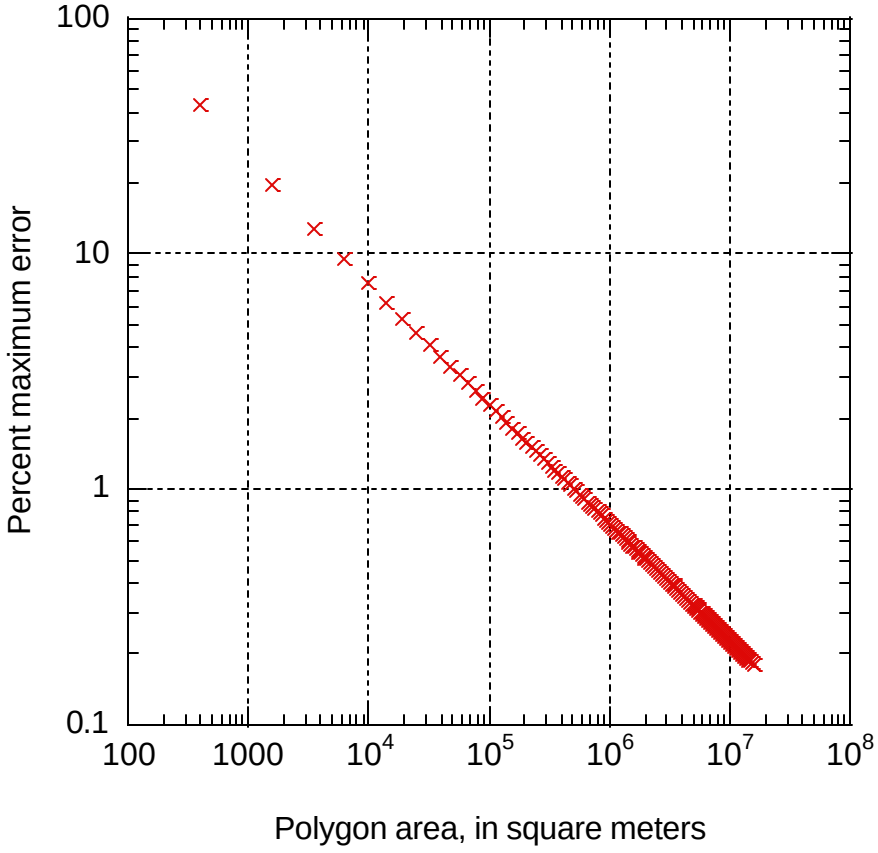


Figure 15- Relationship between the "average shaped" polygons of vairous sizes in the data set used to analyze this reach and percent maximum possible error in reporting their area, as a result of systematic error due to distortion in aerial photographs. Note the diminishing magnitude of error with increasing size of polygon.

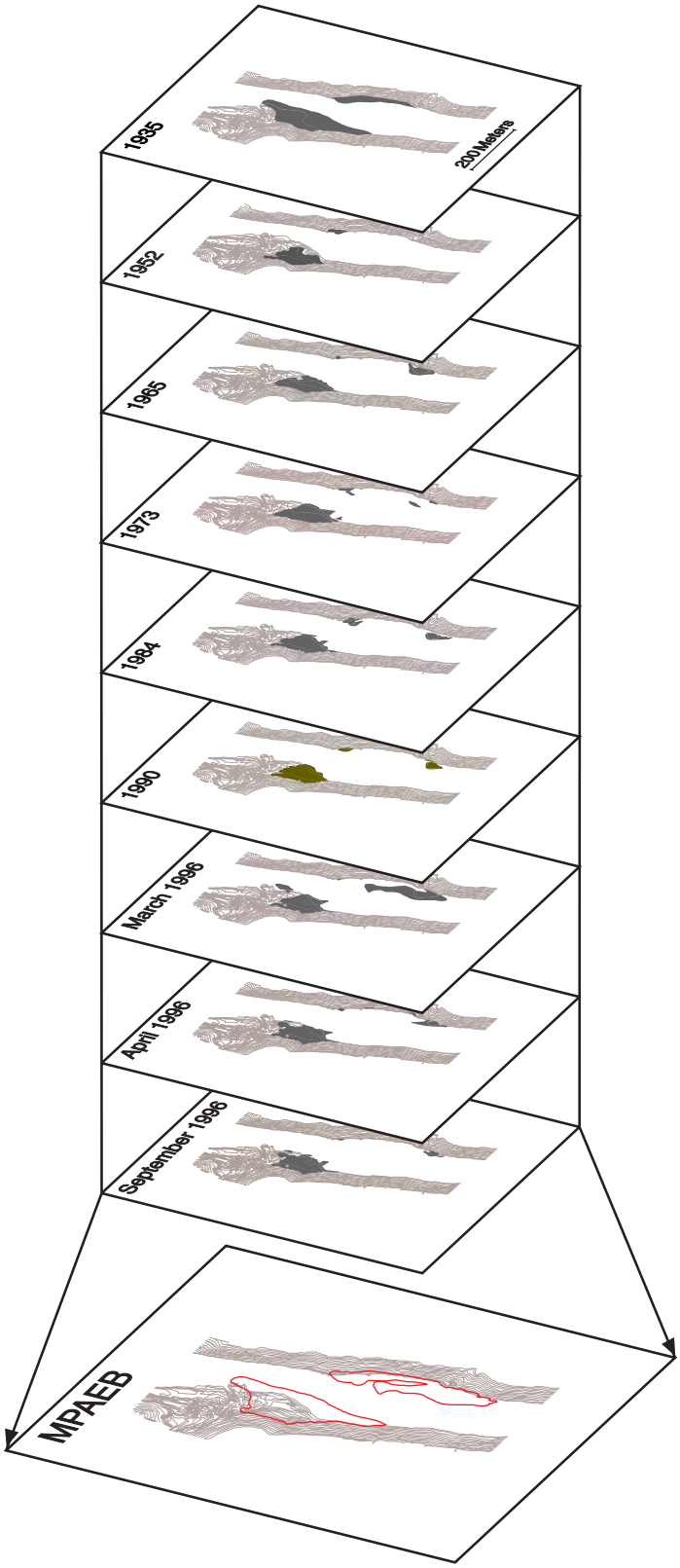


Figure 16- Conceptual model of how maximum potential area of eddy bar (MPAEB) is created.

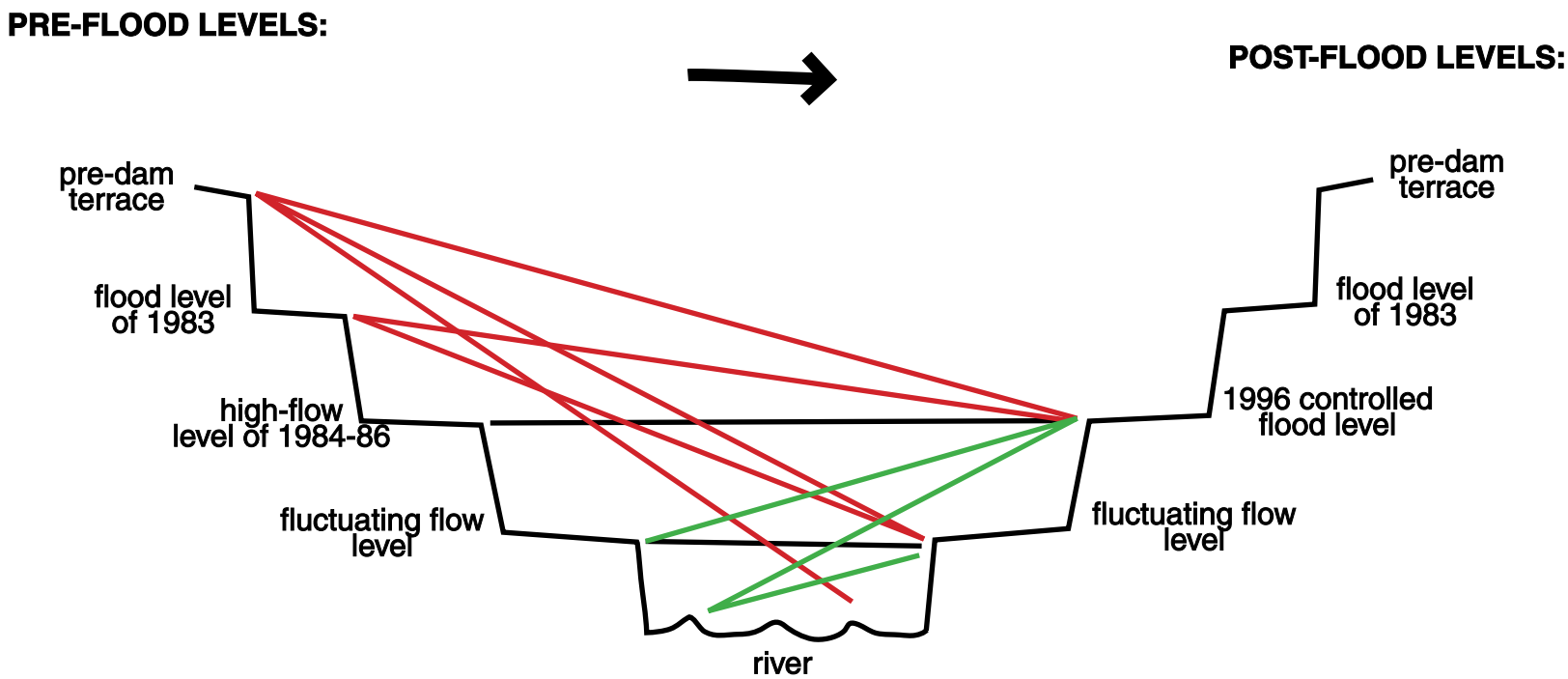


Figure 17- Conceptual model demonstrating the process of determining areas of significant erosion and deposition for the study reach, due to the 1996 controlled flood. Lines indicate the change in levels of map units caused by the flood. Black lines indicate no change from before the flood to after the flood, green lines indicate deposition, and red lines indicate erosion.

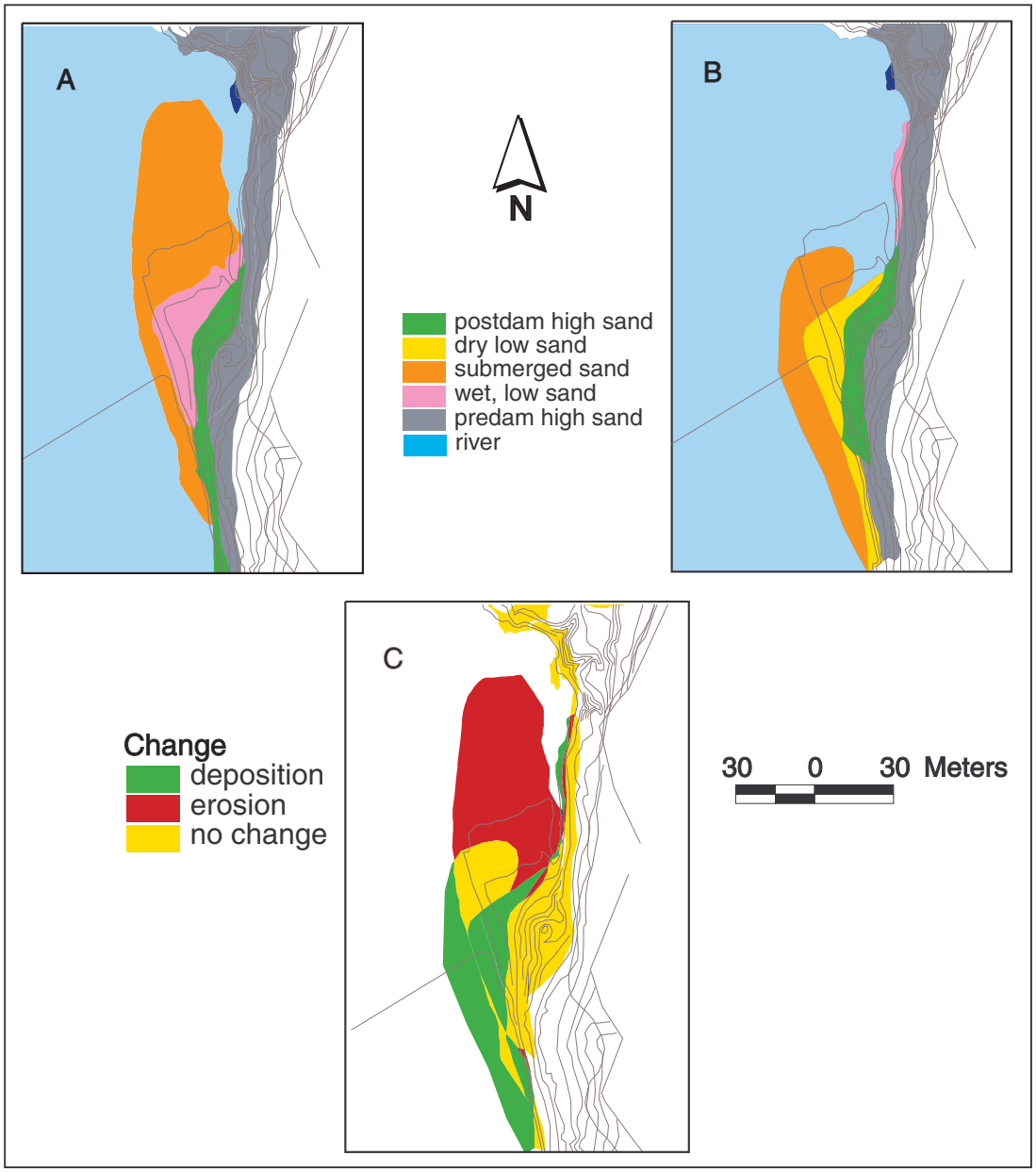


Figure 18- Surficial geologic mapping at a site upstream from Cathedral Wash (A) before, and (B) after the 1996 controlled flood, and (C) the resulting change map.

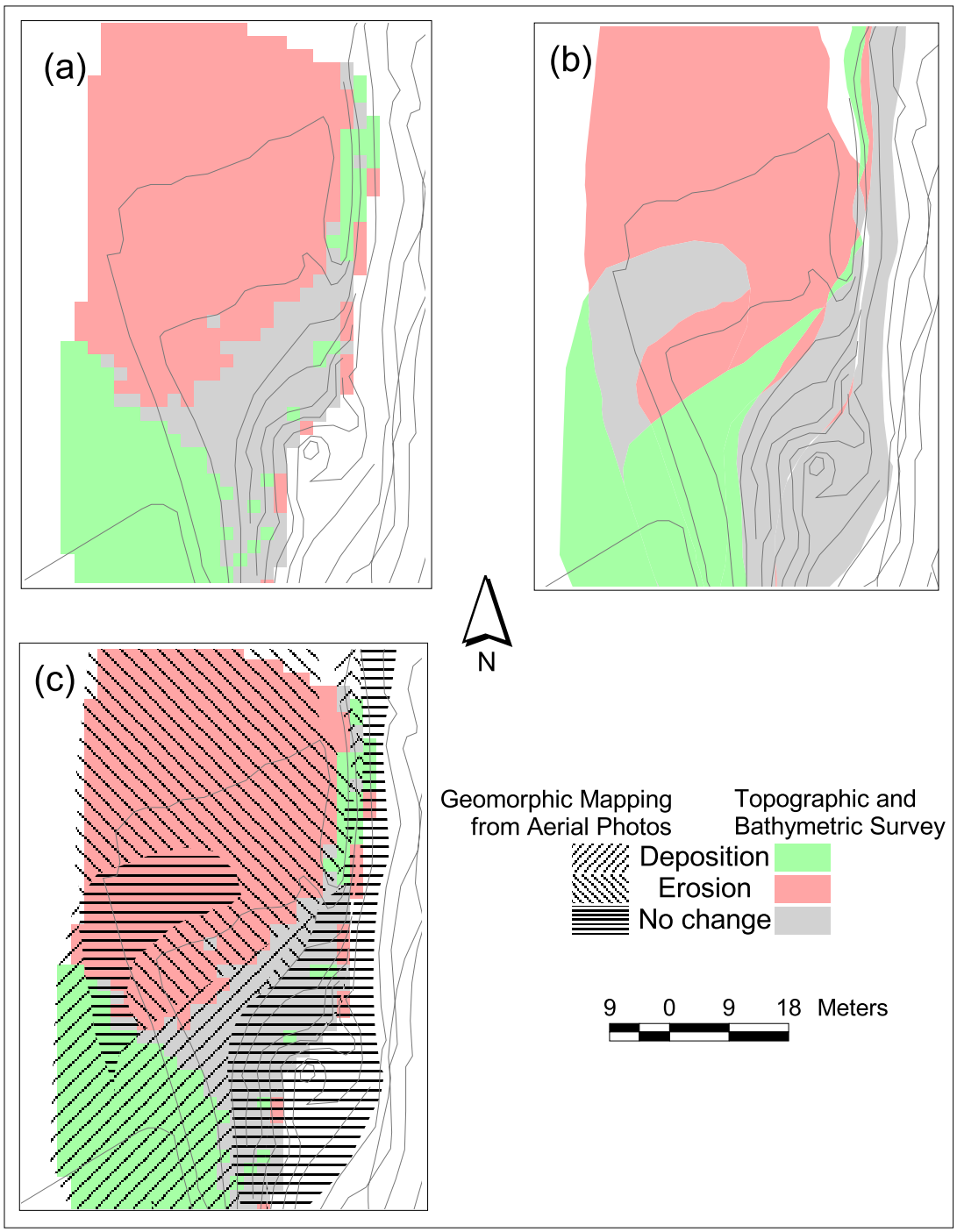


**Figure 19.** Change maps produced from field-based topographic and bathymetric surveys (a), aerial photo interpretation (b), and both maps overlain for comparison (c).

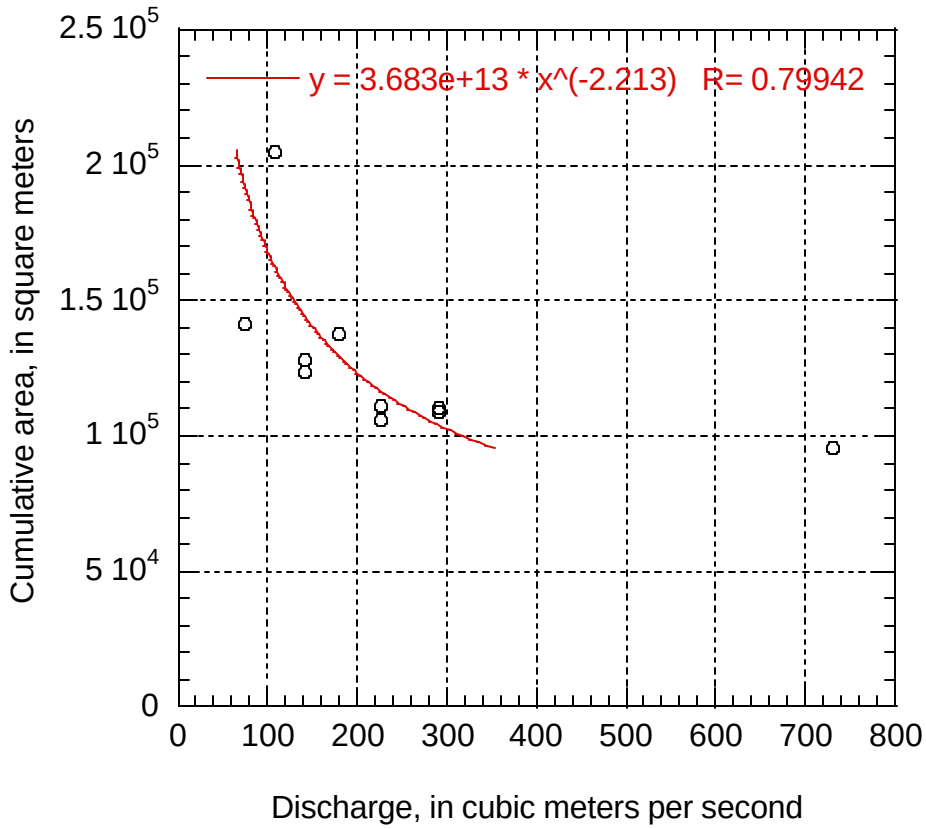


Figure 20- The data points and the curve used for normalization of areas and fill ratios for the study reach. Correlation coefficient for the two axes is 0.80. The points represent the cumulative area of sand within all MPAEB's in the reach for all years of aerial photography (excluding 1951) at known discharges. The reason for the exclusion of 1951 data is that the analysis was complete before the mapping for this year was completed.

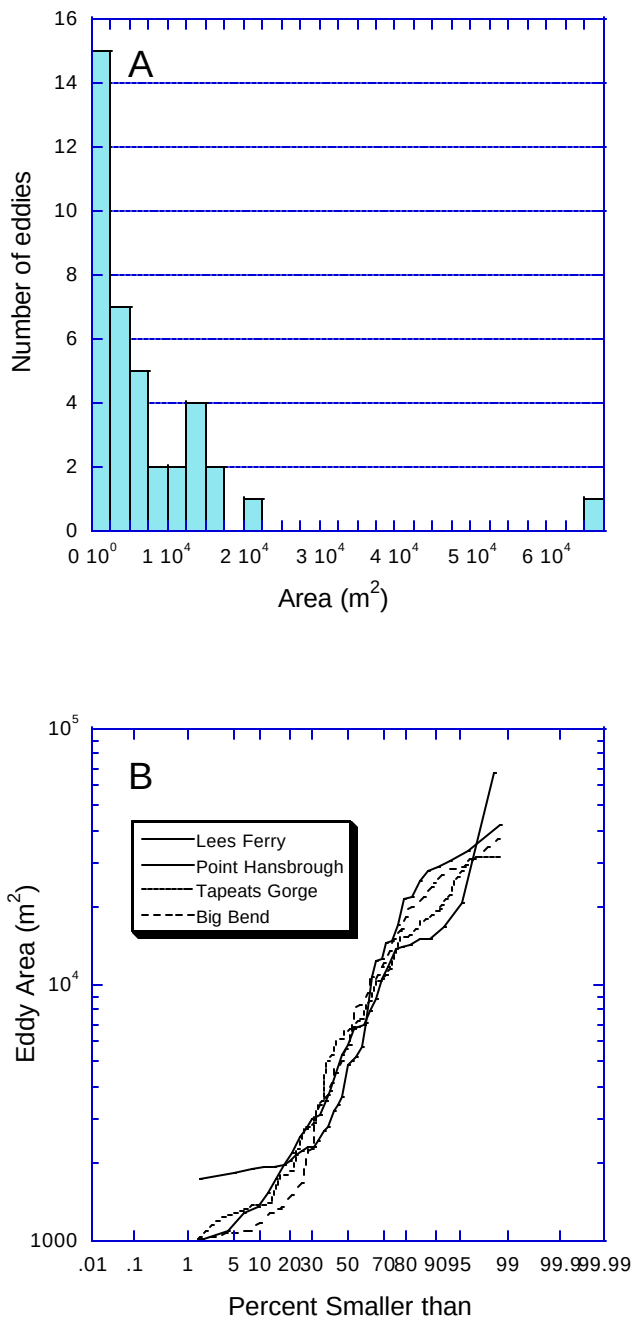


Figure 21- (A) Histogram of size distribution for the MPAEB's in the study reach. (B) Probability curves of size distributions of MPAEB's larger than 1000 $m^2$, in the study reach and reaches analyzed by Schmidt et al. (1999). There are no statistical differences among the distributions of MPAEB sizes.

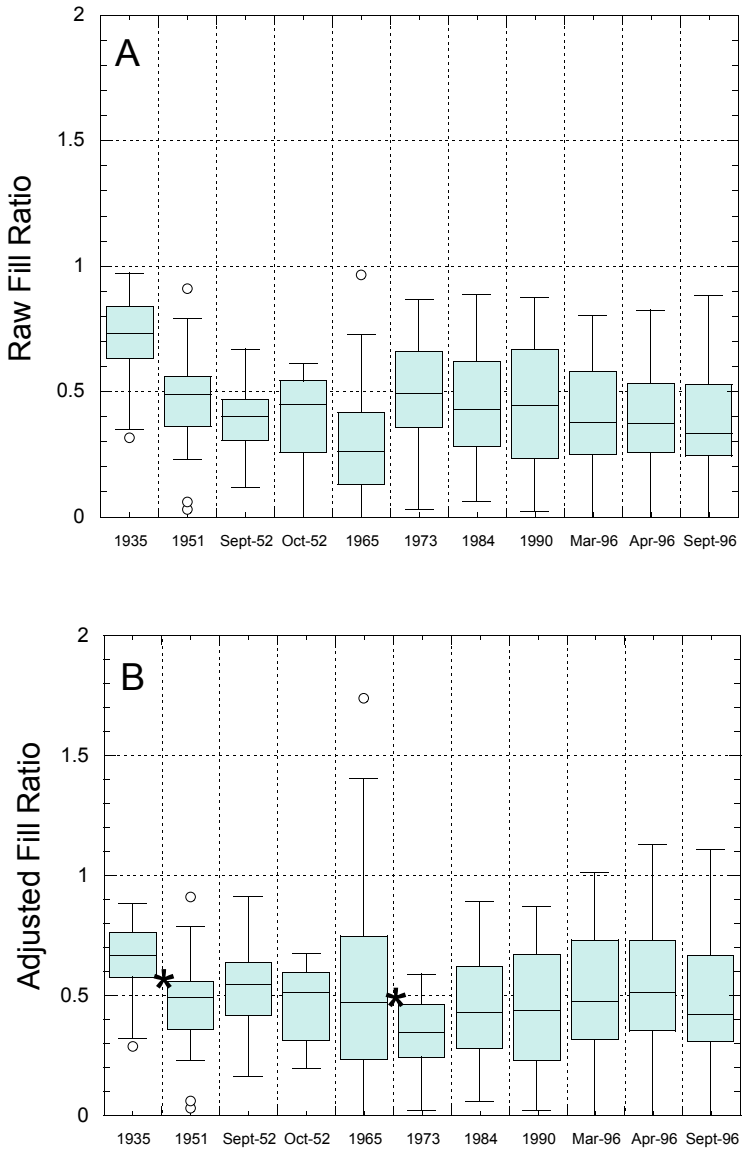


Figure 22- Box plots of raw (A) and adjusted (B) fill ratios for MPAEB's larger than 1000 $m^2$ in the study reach. The boxes represent the upper and lower quartiles of each data set about the median values (50% of the data points); the lines in the boxes indicate the median values; the circles indicate outliers that are farther than 1.5 X interquartile distance from the median; the bars contain all data points that are not outliers. The "*" symbol indicates cases where null hypotheses stating that the distribution of data sets are equal were rejected for 2 adjacent data sets. Statistical tests performed were Mann-WHitney-U tests, with $\alpha = 0.05$.
No statistical analysis was performed on raw fill ratio values because of differences in discharge at time of photography.

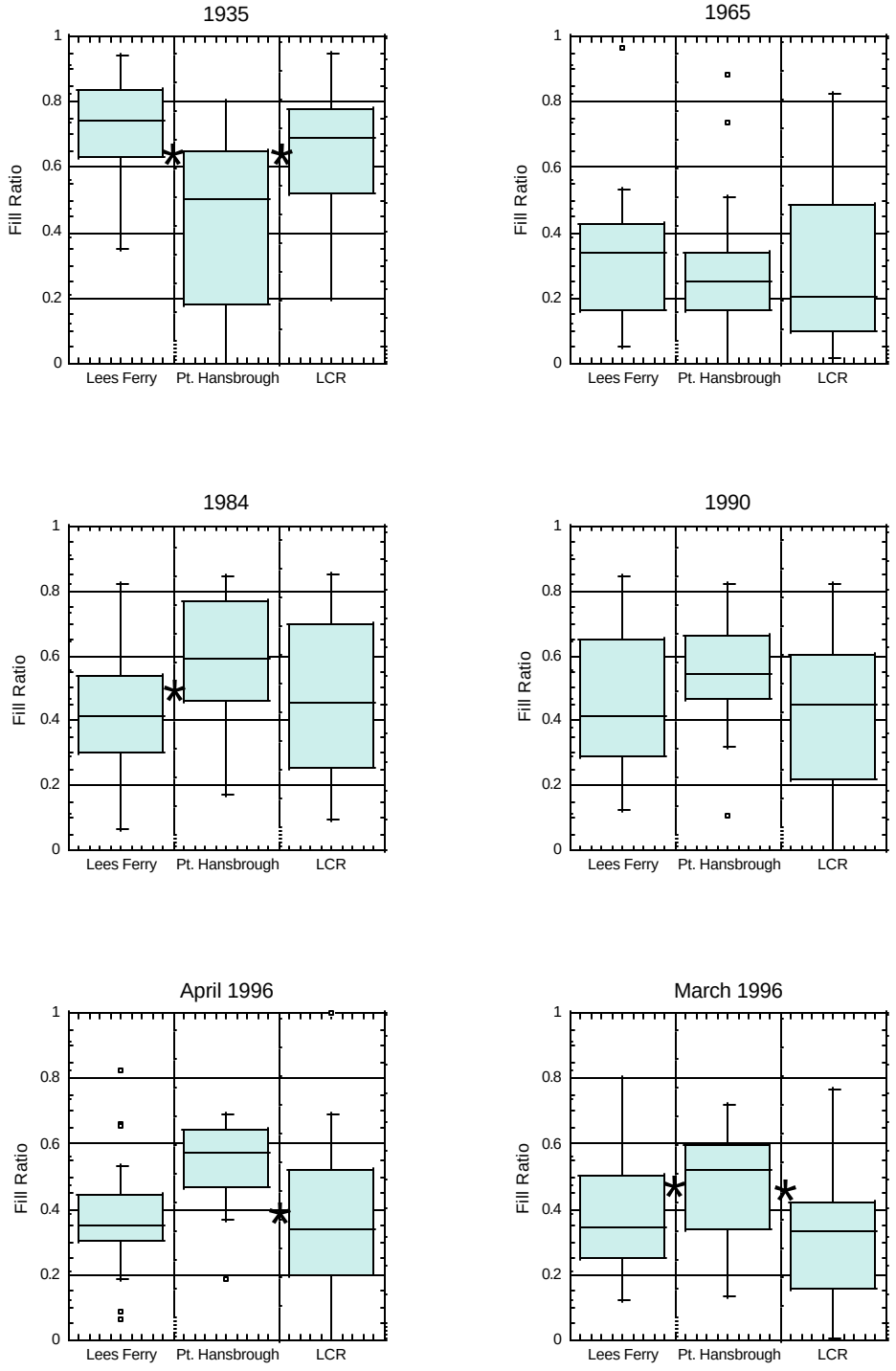


Figure 23- Uncorrected fill ratios for MPAEB's larger than 5000 $m^2$, in the Lees Ferry, Point Hansbrough, and LCR reaches. "*" symbols indicate cases where two adjacent data sets have statistically different distributions. Statistical tests performed were Mann-Whitney-U tests, with $\alpha = 0.05$.

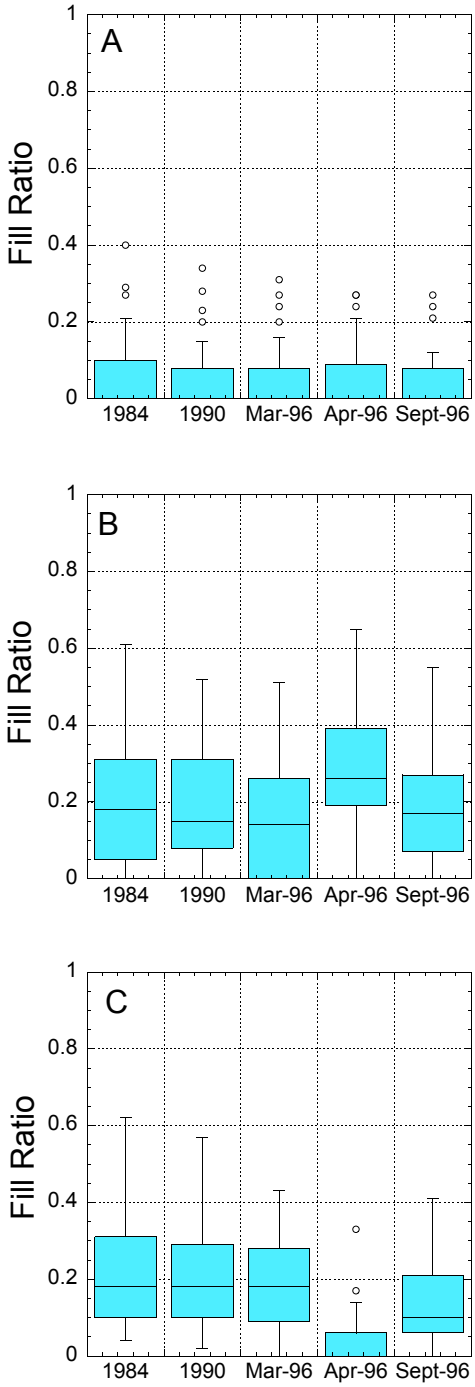


Figure 24- Categorized raw fill ratios for MPAEB's larger than 1000 $m^2$, in the study reach between October 21, 1984 and September 1, 1996. Fill ratio distribution for (A) pre-dam high-elevation deposits, (B) post-dam flood deposits, and (C) power plant level deposits.

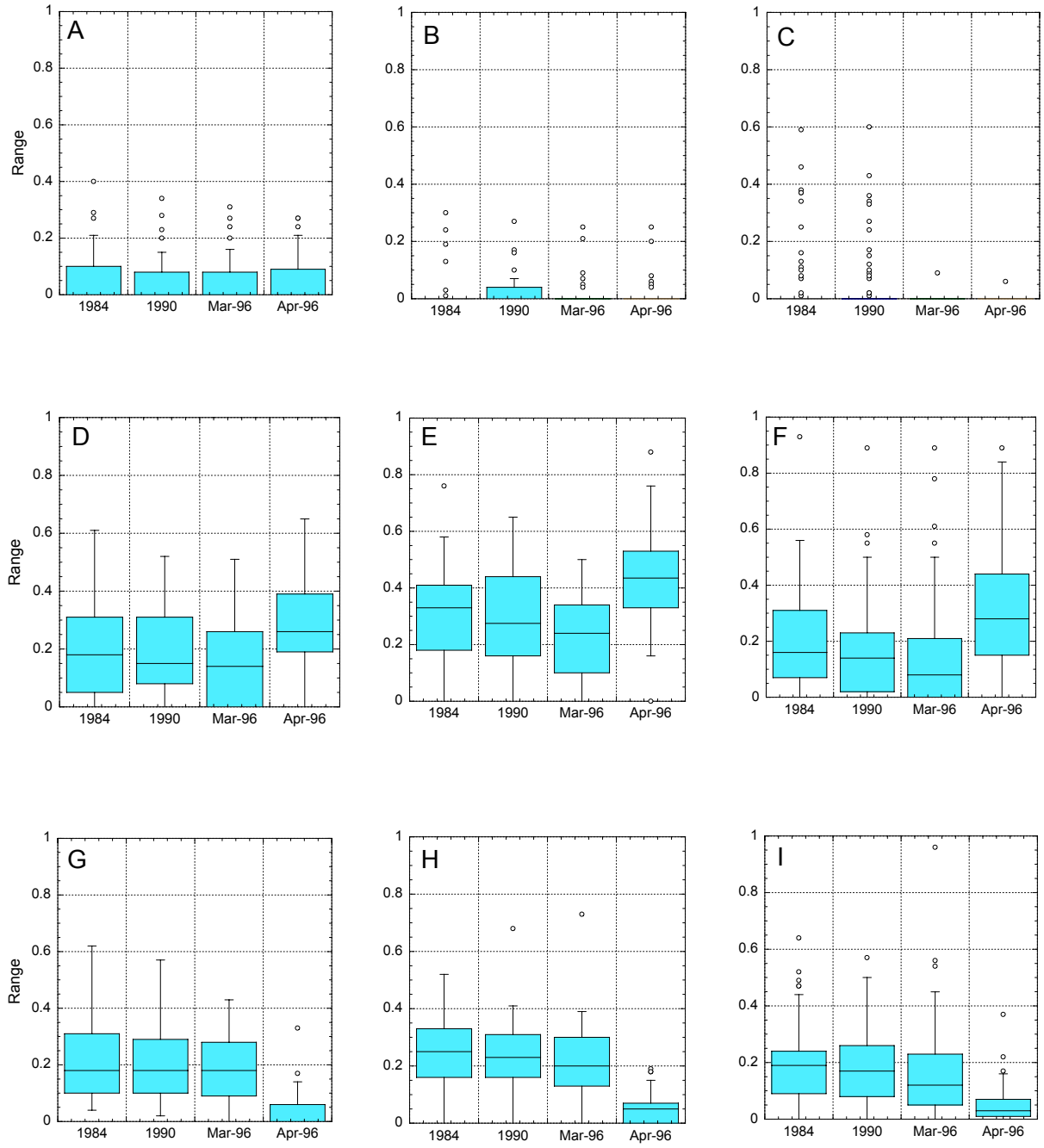


Figure 25- Categorized raw fill ratios for all MPAEB's larger than 1000 $m^2$, for this study reach, and reaches downstream analyzed by Schmidt et al. (1999). The top row shows fill ratios of pre-dam deposits for all reaches, the middle row shows the distribution of post-dam high-elevation deposits, and the bottom row shows the distribution of power plant level deposits.
The left column is data from this study reach, the middle column is from the Point Hansbrough reach, and the right column is from the LCR reach. Table 5 lists the results of statistical analysis of these data.

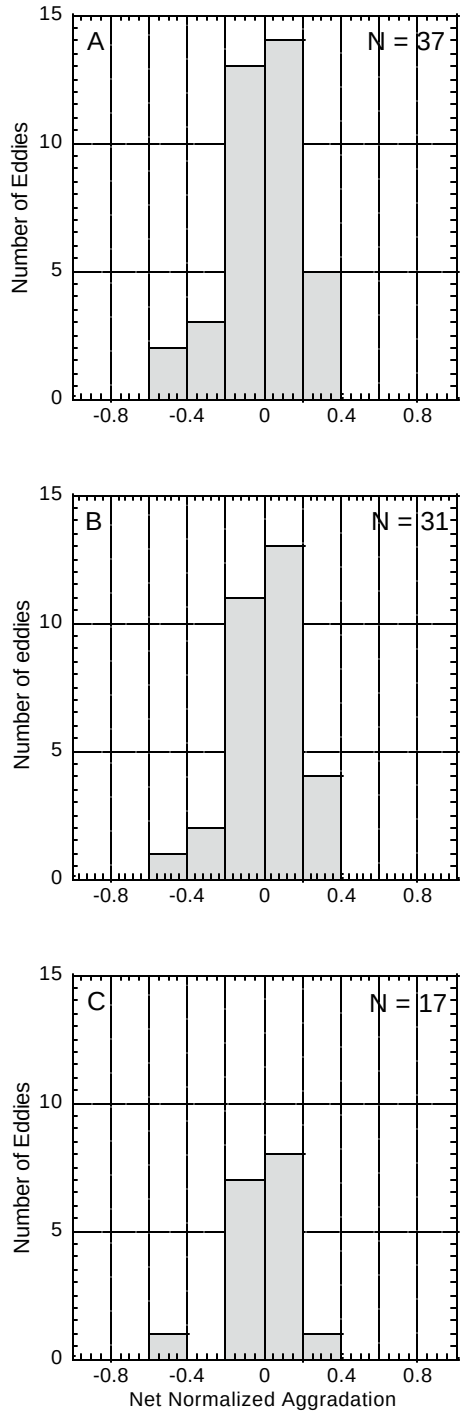


Figure 26 - Net Normalized Aggradation values, for all MPAEB's (A), for MPAEB's larger than1000 $m^2$ (B), for MPAEB's larger than 5000 $m^2$ (C), for the 1996 controlled flood.

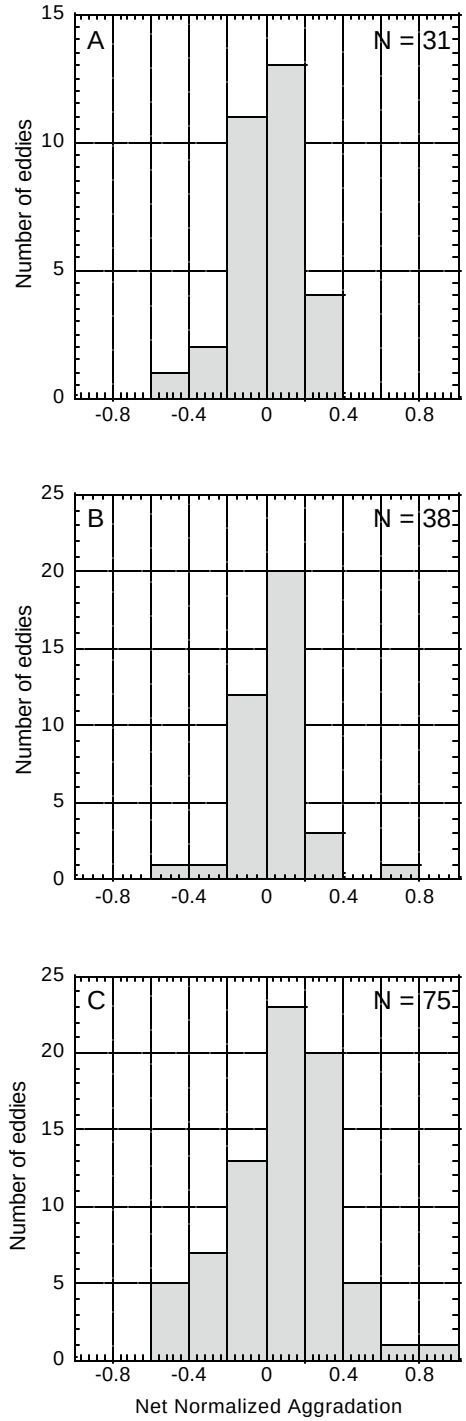


Figure 27- Net normalized aggradation for MPAEB's larger than 1000 $m^2$, for the Lees Ferry reach (A), the Point Hansbrough reach (B), and the LCR reach (C), for the 1996 controlled flood.

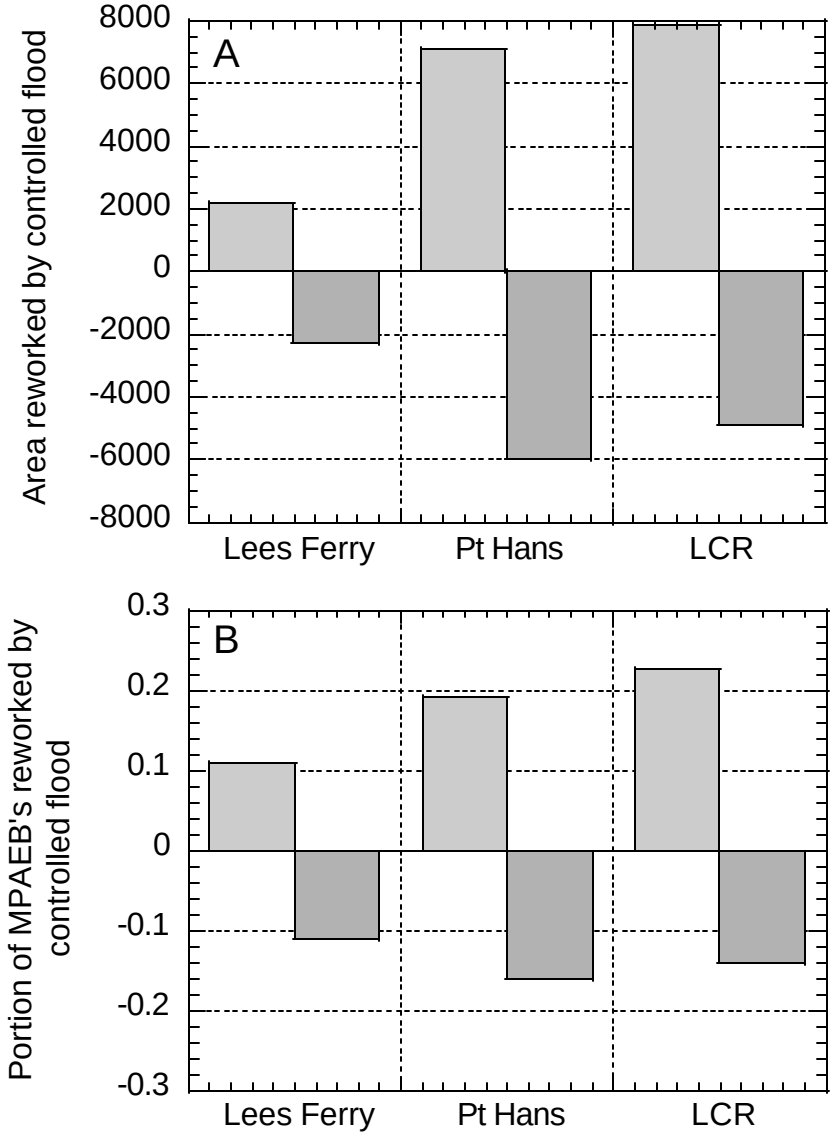


Figure 28- Total areas of significant erosion (horizontal line pattern and with negative values for area) and significant deposition (vertical line pattern and with positive values for area) per river kilometer (A), and per unit area of MPAEB (B) in MPAEB's of our study reach (Lees Ferry) and downstream reaches analyzed by Schmidt et al. (1999), due to the controlled flood of 1996.

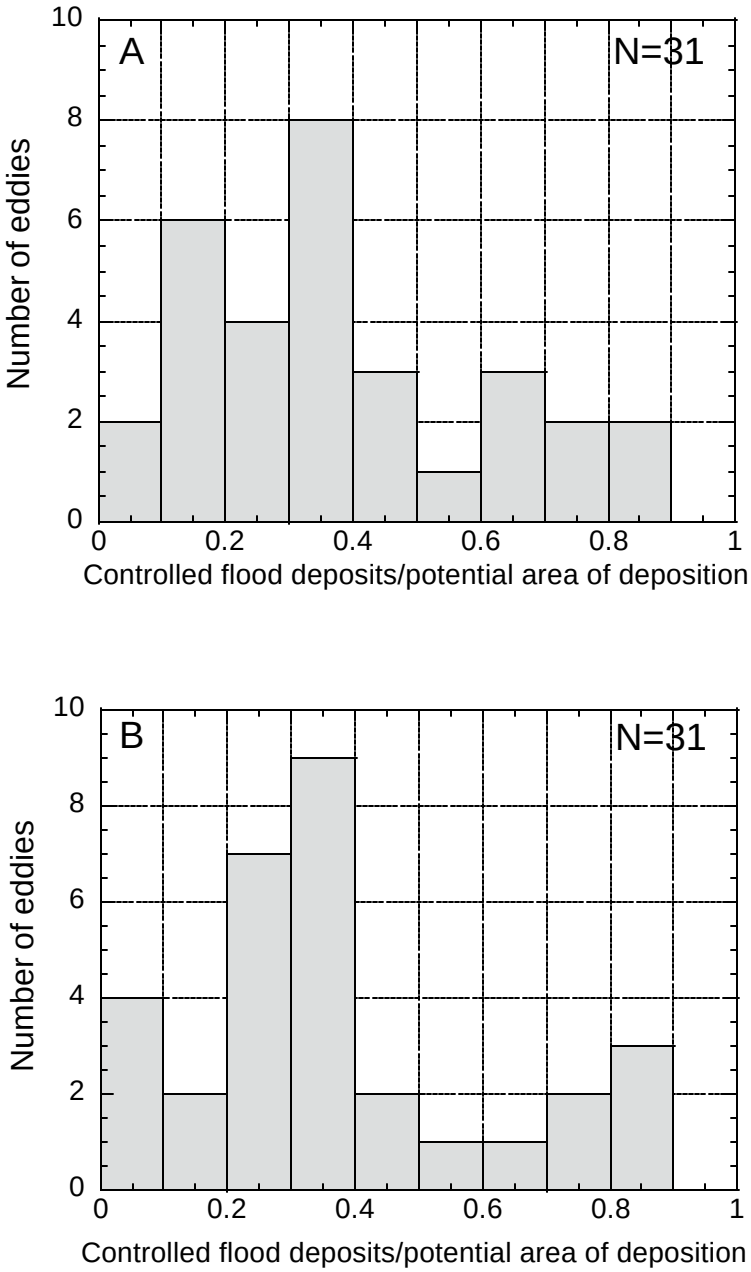


Figure 29- Distribution of the ratios generated by division of total area of sand in each MPAEB by the potential area of deposition, in the study reach, for all MPAEB's larger than 1000 $m^2$ on April 4, 1996 (A), and September 1, 1996 (B).

## REFERENCES CITED


Barrette, J., August, P., Golet, F., 2000, Accuracy assessment of wetland boundary delineation using aerial photography and digital orthophotography, *Photogrammetric Engineering & Remote Sensing*, v. 66, no. 4, p. 409-416.

Burkham, D. E., 1986, Trends in selected hydraulic variables for the Colorado River at Lees Ferry and near Grand Canyon, Arizona, 1922-84: final draft report for the U. S. National Park Service contract No. CX 8000-4-0014.

Grams, P. E., Schmidt, J. C., 1999, Integration of photographic and topographic data to develop temporally and spatially rich records of sand bar change in the Point Hansbrough and Little Colorado River confluence study reaches, Final Report to the Grand Canyon Monitoring and Research Center.

Hazel, J. E., Kaplinski, M., Manone, M. F., Parnell, R. A., Dale, A. R., Ellsworth, J., Dexter, L., 1997, The effects of the 1996 Glen Canyon Dam beach/habitat-building test flow on Colorado River sand bars in Grand Canyon: Final draft report for the U. S. Bureau of Reclamation, Glen Canyon Environmental Studies.

Hazel, J. E., Kaplinski, M., Parnell, R., Manone, M., Dale, A., 1999, Topographic and bathymetric changes at thirty-three long-term study sites, in *The 1996 controlled flood in Grand Canyon, Geophysical Monograph Series,* v. 110, edited by Webb, R. H., Schmidt, J. C., Marzolf, G. R., Valdez, R. A., p. 161-183.

Hereford, R., 1996, Map showing surficial geology and geomorphology of the Palisades Creek area, Grand Canyon National Park, Arizona: *U. S. Geological Survey Miscellaneous Investigations Series Map I-2449,* scale 1:2,000 (with discussion).

Hereford, R., Burke, K. J., Thompson, K. S., 2000, Map showing Quaternary geology and geomorphology of the Lees Ferry area, Arizona, *U. S. Geological Survey Geologic Investigations Series mapI-2663,* scale 1:2,000.

Kearsley, L., Quartaroli, R., 1997, Effects of beach/habitat-building flow on campsites in the Grand Canyon, Final Report to the Grand Canyon Monitoring and Research Center.

Kearsley, L. H., Schmidt, J. C., Warren, K. D., 1994, Effects of Glen Canyon dam on Colorado River sand deposits used as campsites in Grand Canyon National Park, USA: *Regulated Rivers: Research and Management,* v. 9, p. 137-149.

Konieczki, A. D., Graf, J. B., Carpenter, M. C., 1997, Streamflow and sediment data collected to determine the effects of a controlled flood in March and April 1996

on the Colorado River between Lees Ferry and Diamond Creek, Arizona: *U. S. Geological Survey Open-File report,* 97-224, 55 p.

Korman, J., Walters, C., 1998, User's guide to the Grand Canyon ecosystem model, prepared for the Grand Canyon Monitoring and Research Center.

Lazorchak, J. M., Klemm, D. J., Peck, D. V., 1998, Environmental Monitoring and Assessment Program-Surface Waters: Field Operations and Methods for Measuring the Ecological Condition of Wadeable Streams, Research Triangle Park, NC: National Exposure Research Laboratory and National Health and Environmental Effects Research Laboratory, Office of Research and Development, U.S. Environmental Protection Agency.

Mulder, B. S., Noon, B. R. Spies, T. A., Raphael, M. G., Palmer, C. J., Olsen, A. R., Reeves, G. H., Welsh, H. H., 1999, The Strategy and Design of the Effectiveness Monitoring Program for the Northwest Forest Plan, U. S. Department of Agriculture, Forest Service, Pacific Northwest Research Station, Portland, Oregon, 138 p.

National Research Council, 1996, *Downstream: adaptive management of Glen Canyon Dam and the Colorado River ecosystem*, National Academy Press, Washington, D. C.

Pemberton, E. L., 1976, Channel change in the Colorado River below the Glen Canyon Dam: Proceedings of the third federal inter-agency sedimentation conference (Sedimentation Committee of the Water Resource Council), v. 5, p. 61-73.

Rubin, D. M., Schmidt, J. C., Moore, J. N., 1990, Origin, structure, and evolution of a reattachment bar. Colorado River, Grand Canyon, Arizona, *Journal of Sedimentary Petrology,* 60, p. 982-991.

Rubin, D. M., Nelson, J. M., Topping, D. J., 1998, Relation of inversely graded deposits to suspended-sediment grain-size evolution during the 1996 flood experiment in Grand Canyon: *Geology*, v. 26, no. 2, p. 99-102.

Schmidt, J. C., 1990, Recirculating flow and sedimentation in the Colorado River in Grand Canyon, Arizona: *Journal of Geology*, v. 98, p. 709-724.

Schmidt, J. C., 1999, Summary and synthesis of geomorphic studies conducted during the 1996 controlled flood in Grand Canyon, in *The 1996 controlled flood in Grand Canyon, Geophysical Monograph Series,* v. 110, edited by Webb, R. H., Schmidt, J. C., Marzolf, G. R., Valdez, R. A., p. 1-21.

Schmidt, J. C., Graf, J. B., 1990, Aggradation and degradation of alluvial sand deposits, 1965 to 1986, Colorado River, Grand Canyon National Park, Arizona: *U. S. Geological Survey , Professional Paper 1493.*

Schmidt, J. C., Grams, P. E., Leschin, M. F., 1999, Variation in the magnitude and style of deposition in three long (8-12km) reaches as determined by photographic analysis, in *The 1996 controlled flood in Grand Canyon, Geophysical Monograph Series,* v. 110, edited by Webb, R. H., Schmidt, J. C., Marzolf, G. R., Valdez, R. A., p. 185-204.

Schmidt, J. C., Grams, P. E., Webb, R. H., 1995, Comparison of the magnitude of erosion along two large regulated rivers, *Water Resources Bulletin*, v. 31, no. 4, p. 617-631.

Schmidt, J. C., Leschin, M. F., 1995, Geomorphology of post-Glen Canyon Dam fine-grained alluvial deposits of the Colorado River in Point Hansbrough and Little Colorado River confluence study reaches in Grand Canyon National Park, Arizona: final draft report for the U. S. Bureau of Reclamation, Glen Canyon Environmental Studies.

Schmidt, J. C., Rubin, D. M., 1995, Regulated streamflow, fine-grained deposits, and effective discharge in canyons with abundant debris fans: *Geophysical Monograph*, v. 89, p. 177-194.

Suter, G. W., 1993, Ecological Risk Assessment, Lewis Publishers, Chelsea, Michigan.

Topping, D. J., Rubin, D. M., Vierra, L. E., 2000a, Colorado River sediment transport: 1. Natural supply limitation and the influence of Glen Canyon Dam, *Water Resources Research,* v. 36, no. 2, p. 515-542.

Topping, D. J., Rubin, D. M., Nelson, J. M., Kinzel, P. J., Corson, I. C., 2000b, Colorado River sediment transport: 2. Systematic bed-elevation change and grain-size effects of sand supply limitation, *Water Resources Research,* v. 36, no. 2, p. 543-570.

U. S. Department of the Interior, 1995, Final Environmental Impact Statement, Operation of Glen Canyon Dam, Colorado River, Storage Project, Coconino County, Arizona, 337 p., Bureau of Reclamation, Salt Lake City, Utah.

Webb, R. H., Wegner, D. L., Andrews, E. D., Valdez, R. A., Patten, D. T., 1999, Downstream effects of Glen Canyon Dam on the Colorado River in Grand Canyon: a review, in *The 1996 controlled flood in Grand Canyon, Geophysical Monograph Series,* v. 110, edited by Webb, R. H., Schmidt, J. C., Marzolf, G. R., Valdez, R. A., p. 1-21.

Wiele, S. M., Andrews, E. D., Griffin, E. R., 1999, The effect of sand concentration on depositional rate, magnitude, and location in the Colorado River below the Little Colorado River, in *The 1996 controlled flood in Grand Canyon, Geophysical*

*Monograph Series,* v. 110, edited by Webb, R. H., Schmidt, J. C., Marzolf, G. R., Valdez, R. A., p. 131-145.

## APPENDIX A
## MAP UNIT DESCRIPTIONS

Two separate criteria are used to describe the surficial deposits mapped. These are type and level, and are described below in detail. Each of these are implemented as separate attribute classes in the polygon attribute tables of the GIS coverages. These designations are based on those used by Hereford (1996), Schmidt and Leschin (1995), Schmidt et al. (1999), Grams and Schmidt (1999), Hereford et al. (2000). However, detailed descriptions are specific to the study reach between Lees Ferry and Badger Creek Rapid.

### Type:

The main focus of mapping for this project has been on fine-grained deposits of the mainstem of the Colorado River in this reach. However, deposits formed by processes other than mainstem flow, such as tributary debris flows are also mapped in all 1996 photo-series.

### ALLUVIUM

**sb** **Separation bar;** very fine to fine-grained sediments immediately downstream from constrictions caused by debris fans or talus cones. This is the upstream end of the expansion in the channel where main flow separates from the channel wall and an eddy is formed. The upstream end of a separation bar is typically highest topographically.

**rb** **Reattachment bar;** fine-grained deposits near the downstream end of the expansion downstream from a constriction where main flow rejoins the channel wall. There is usually a return current channel on the shoreward side of the deposit. The downstream end of these deposits are generally topographically higher. In some cases subaqueous bedforms are observed.

**eb** **Undifferentiated eddy bar;** fine-grained sediments deposited in eddy complexes. This designation is used in places where separation and reattachment bars cannot be differentiated or this differentiation is unnecessary. Lack of ability to differentiate is mainly due to the fact that in some cases separation and reattachment bars blend into one another. This can cause a deposit not to have distinguishing characteristics, and only be recognizable as an eddy deposit due to its location in a channel expansion immediately downstream from a constriction.

**cm** **Channel margin deposit;** fine-grained deposits in long narrow bands parallel to the river, near the water's edge. These deposits have levee topography in places. For the purposes of simplicity, submerged and also mid-channel deposits that are obviously not eddy deposits have been

called channel margin deposits as well. In some cases (e.g., April 4, 1996) bedforms such as dunes and ripples are observed.

**gv** **Gravel;** unconsolidated clasts ranging in size from cobbles to boulders, in some cases including very coarse sand matrix. Clasts are sub-rounded to rounded, with Paleozoic sedimentary lithology. These deposits are in the form of mid-channel or channel margin bars, often occurring downstream from tributary debris fans and referred to as rock gardens. These gravels are typically reworked clasts introduced to the river by tributary debris fans, and therefore the lithology of their clasts is generally consistent with that of the upstream debris fan.

**ts** **Tributary sand;** fine-grained deposits ranging in size from coarse sand to silt and clay, white to reddish brown in color, usually deposited in the most recent flash flood of an ephemeral tributary. These deposits generally appear darker than mainstem fine-grained deposits nearby and are generally coarser and poorly sorted. The exception is the deposits of the Paria River. These are composed of very fine sand to silt and clay, and are white in color, very similar in appearance to mainstem deposits.

## COLLUVIUM

**df** **Debris fan;** very poorly sorted material ranging is size from cobbles to large boulders, derived from local sedimentary rocks of Paleozoic age, intermixed with reddish matrix. The clasts are angular to sub-angular, made up mainly of sandstone, shale, mudstone, and limestone. These deposits occur near mouths of tributaries and form distinctly shaped cones.

**talus** **Talus;** cobble to boulder sized angular deposits at bases of cliffs; derived from these cliffs, therefore of the same Triassic and Permian lithology.

**rock** **Boulder;** these are boulders large enough to be recognized when viewed stereoscopically on aerial photos. They are usually very angular in appearance and can be classified as talus. The only reason for a separate designation is the fact that they are individual boulders surrounded by water, some of which have been used as ground control points in the process of digitizing the mapping into a GIS database.

### EOLIAN DEPOSITS

**es** **Eolian sand;** fine-grained sand deposited and/or reworked by wind. These deposits typically are found with dune features. They are also usually topographically higher than **fs** deposits, and therefore have not been inundated in the post-dam era. Since these deposits are not of

interest for analyses mentioned herein, they have the level designation **NA**.

**Level:**

The level designations used in mapping and described below have a different meaning for coarse deposits than they do for fine-grained deposits. In the case of fine-grained deposits they denote depositional or reworked surfaces therefore they indicates the formative discharge range. In other words, these surfaces represent the minimum water stage during deposition or reworking by a particular range of discharge. In the case of coarse-grained deposits, the level designation only indicates that the deposit was inundated by a particular range of discharge. These discharges generally are not capable of moving the grains making up the deposit.

**For photo-series from10/21/1984 and later**

**ff** **Fluctuating flow level (1984-1996; formative discharge: 890 $m^3$/sec or less);** these are deposits that are inundated by flows caused by daily fluctuations in releases from Glen Canyon Dam. They are coarse- to fine-grained sand, sometimes silty, ranging in color from light gray to red. Deposits can have a thickness of up to 1 m. **ff** deposits are usually between **hf** or **ef** which are higher, and the river or **ff(w)** or **ff(sub)** which are lower and sloping towards the river. Sometimes there is a single cutbank between the deposit and the river; more often, however, there is a subtle break in slope. These deposits appear white in all years of photography visible, and have minimal vegetation cover due to constant reworking.

**ff(w)** **Fluctuating flow level (wet) (1984-1996);** these deposits were still wet from lowering of release from the dam so aerial photos could be flown. They are made up of coarse to fine, and sometimes silty sand. These deposits are inundated by daily fluctuations in discharge and appear darker than **ff** deposits in photos. They are usually between **ff** and **ff(sub)** deposits, which are topographically higher and lower respectively. There is no topographic break in slope present between **ff(w)** and **ff** deposits; they grade into one another and are the same depositional/reworked surface.

**ff(sub)** **Fluctuating flow level (submerged) (1984-1996);** these deposits were below the water surface at time of photography. These are similar in composition to **ff** and **ff(w)** deposits. Observation of these deposits in aerial photos is dependent on time of day (sun angle) and clarity of water. These are the lowest topographic fine-grained deposits mapped in the reach.

**hf** **High flow level (1984-1986; formative discharge: 890-1400 $m^3$/sec);** deposits of the high flows of 1984-1986. Fine-grained deposits as observed in aerial photos of Oct 21, 1984, and June 2, 1990. The photo-series from 1984 are the most useful tool in mapping these deposits. **hf** deposits in these photos appear clean and gray, slightly darker than adjacent, topographically lower **ff** deposits. Vegetation growing from these surfaces are often bent down by water during very recent inundation, making it possible to differentiate these surfaces from the nearby and topographically higher **fs** deposits, which also have fresh looking surfaces. The direction in which the vegetation is bent was used to determine dominant flow direction during inundation, therefore indicating deposit type in some cases. These deposits have not been observed in the field. All known deposits of this category were reworked in the reach by the controlled flood of 1996. Deposits identified as **hf** are typically between **fs** and **ff** deposits.

**fs** **Flood stage level (1983; formative discharge: 1400-2700 $m^3$/sec);** deposited by high dam releases of 1983, **fs** deposits are the highest topographic surface inundated since the closure of Glen Canyon Dam. They are poorly sorted, medium to coarse sand. The topographic and stratigraphic position of **fs** deposits is between **hf**, and **htt** or ht deposits. They appear very similar to **hf** deposits aerial photos, and can easily be confused with them. An **fs** surface is most easily differentiated by a cutbank between it and an **hf** surface.

**htt** **Pre-dam high Tamarisk terrace (prior to 1963; formative discharge: greater than 2700 $m^3$/sec);** this is a pre-dam terrace that has not been inundated in the post-dam era. These deposits are made up of well sorted, fine sand to silt and clay. Their surfaces are typically covered with Tamarisk in all post-dam photo-series. The tamarisk has helped to stabilize these deposits in many places. These deposits are topographically higher than the **fs** level deposits.

**ht** **Pre-dam high terrace (prior to 1963; formative discharge: greater than 2700 $m^3$/sec);** high elevation pre-dam terraces not inundated in the post-dam era, and are topographically the highest deposits in the reach. These deposits are made up of well sorted, muddy, fine sand, often having well-preserved depositional structures due to cementing. These terraces have several different sub-levels, representing several depositional events; they are generally higher topographically than the **htt** level. Although generally free of vegetation, in many places shrubby plants such as sagebrush are growing out of these surfaces.

**ef** **Controlled flood level (1996; formative discharge: 890-1270 $m^3$/sec);** deposits of the controlled flood in spring of 1996. These are moderately sorted coarse to medium, sometimes muddy sand. Color ranges from white to light pink or gray. In aerial photos these deposits appear white or light gray and are recognized by being slightly darker than adjacent **ff** deposits, and sometimes having vegetation bent down.

**NA** **Not applicable;** this level designation is used when level of inundation is not recognizable, or the formative processes are not fluvial, such as tributary debris fans and talus. It is also used for fine-grained deposits altered by tributary flow or eolian processes.

**Photo-series before 10/21/1984**

**c** **Clean sand;** dry clean fine-grained deposits low in elevation. These deposits are bare and free of vegetation. They are probably deposits associated with the most recent inundation of the area. In all photo series they appear white and free of vegetation. In photos of 1935 and 1952, several sub-levels are visible, which suggest more than one recent inundation with variation in discharge. In the photo-series from 1965 and 1973 this level appears as narrower strips of sand. There is a high probability that in these photo-series the low-lying deposits were maintained/reworked by daily fluctuation in discharge due to fluctuations in dam releases. These deposits are higher than those mapped as **w** and lower than those mapped as **u**.

**w** **Wet sand;** low-lying fine-grained deposits still wet from the most recent inundation. These deposits are near the river and therefore topographically the lowest of the fine-grained deposits mapped. They are just above the water surface and lower than the **c** level. They appear medium to dark gray in all photo-series mapped, due to the moisture content.

**u** **Upper; younger pre-dam deposits;** deposits not inundated until the post-dam floods of 1983-1986 and 1996. These deposits appear light gray in all photo-series mapped. They appear darker than adjacent or nearby **c** level deposits. These deposits were reworked by the infrequent post-dam floods to form the **hf** and **fs** levels. They are higher than **c** and lower than **u2** deposits, if both are present adjacent to these deposits.

**u2** **Upper; older pre-dam deposits;** high elevation deposits that probably have not been inundated since closure of Glen Canyon Dam. Most of these deposits correlate to the **ht** and **htt** levels mapped in the photo-series of 1984 and later. These deposits appear free of vegetation in aerial photos of 1935. In the 1952 photo-series several tamarisk trees appear to have been established on these surfaces.

APPENDIX B- AML used to produce coverage of MPAEB

```
&args yr35cv yr52acv yr52bcv yr65cv yr73cv yr84cv yr90cv yr96acv yr96bcv yr96ccv
output

/*Program to compute eddy complex boundaries from multiple years of maps
/*Included sb rb and eb as eddy bars

/*Checks for proper command line entry
&if ^ [exists %yr35cv% -cover] &then &do
  &type %yr35cv% does not exist...
  &type Usage:  &r complex2 <1935 cover> <sept52 cover> <oct52 cover> <1965
cover> <1973 cover> <1984 cover> <1990 cover> <1996 pre cover> <1996 post-a
cover> <1996 post-b cover> <output cover>
  &return
&end
&if ^ [exists %yr52acv% -cover] &then &do
  &type %yr52acv% does not exist...
  &type Usage:  &r complex2 <1935 cover> <sept52 cover> <oct52 cover> <1965
cover> <1973 cover> <1984 cover> <1990 cover> <1996 pre cover> <1996 post-a
cover> <1996 post-b cover> <output cover>
  &return
&end
&if ^ [exists %yr52bcv% -cover] &then &do
  &type %yr52bcv% does not exist...
  &type Usage:  &r complex2 <1935 cover> <sept52 cover> <oct52 cover> <1965
cover> <1973 cover> <1984 cover> <1990 cover> <1996 pre cover> <1996 post-a
cover> <1996 post-b cover> <output cover>
  &return
&end
&if ^ [exists %yr65cv% -cover] &then &do
  &type %yr65cv% does not exist...
  &type Usage:  &r complex2 <1935 cover> <sept52 cover> <oct52 cover> <1965
cover> <1973 cover> <1984 cover> <1990 cover> <1996 pre cover> <1996 post-a
cover> <1996 post-b cover> <output cover>
  &return
&end
&if ^ [exists %yr73cv% -cover] &then &do
  &type %yr73cv% does not exist...
  &type Usage:  &r complex2 <1935 cover> <sept52 cover> <oct52 cover> <1965
cover> <1973 cover> <1984 cover> <1990 cover> <1996 pre cover> <1996 post-a
cover> <1996 post-b cover> <output cover>
  &return
&end
&if ^ [exists %yr84cv% -cover] &then &do
  &type %yr84cv% does not exist...
```

```
  &type Usage:  &r complex2 <1935 cover> <sept52 cover> <oct52 cover> <1965
cover> <1973 cover> <1984 cover> <1990 cover> <1996 pre cover> <1996 post-a
cover> <1996 post-b cover> <output cover>
  &return
&end
&if ^ [exists %yr90cv% -cover] &then &do
  &type %yr90cv% does not exist...
  &type Usage:  &r complex2 <1935 cover> <sept52 cover> <oct52 cover> <1965
cover> <1973 cover> <1984 cover> <1990 cover> <1996 pre cover> <1996 post-a
cover> <1996 post-b cover> <output cover>
  &return
&end
&if ^ [exists %yr96acv% -cover] &then &do
  &type %yr96acv% does not exist...
  &type Usage:  &r complex2 <1935 cover> <sept52 cover> <oct52 cover> <1965
cover> <1973 cover> <1984 cover> <1990 cover> <1996 pre cover> <1996 post-a
cover> <1996 post-b cover> <output cover>
  &return
&end
&if ^ [exists %yr96bcv% -cover] &then &do
  &type %yr96bcv% does not exist...
  &type Usage:  &r complex2 <1935 cover> <sept52 cover> <oct52 cover> <1965
cover> <1973 cover> <1984 cover> <1990 cover> <1996 pre cover> <1996 post-a
cover> <1996 post-b cover> <output cover>
  &return
&end
&if ^ [exists %yr96ccv% -cover] &then &do
  &type %yr96ccv% does not exist...
  &type Usage:  &r complex2 <1935 cover> <sept52 cover> <oct52 cover> <1965
cover> <1973 cover> <1984 cover> <1990 cover> <1996 pre cover> <1996 post-a
cover> <1996 post-b cover> <output cover>
  &return
&end

/*Places files together for analysis
union %yr35cv% %yr52acv% zztemp1 .000001 join
union zztemp1 %yr52bcv% zztemp2 .000001 join
union zztemp2 %yr65cv% zztemp3 .000001 join
union zztemp3 %yr73cv% zztemp4 .000001 join
union zztemp4 %yr84cv% zztemp5 .000001 join
union zztemp5 %yr90cv% zztemp6 .000001 join
union zztemp6 %yr96acv% zztemp7 .000001 join
union zztemp7 %yr96bcv% zztemp8 .000001 join
union zztemp8 %yr96ccv% zztemp9 .000001 join

/*Adds new attributes for computing change
```

```
additem zztemp9.pat zztemp9.pat ebid 4 4 I

/*Selects eddy bars from yr96a
&data arc info
  ARC
  SEL ZZTEMP9.PAT
  MOVE '0' TO EBID
  RES T-PRE CN 'b'
  MOVE '1' TO EBID
  AS
/*Selects eddy bars from yr96b
  RES T-POST CN 'b'
  MOVE '1' TO EBID
  AS
/*Selects eddy bars from yr96c
  RES T-APOST CN 'b'
  MOVE '1' TO EBID
  AS
/*Selects eddy bars from yr84
  RES T-84 CN 'b'
  MOVE '1' TO EBID
  AS
/*Selects eddy bars from yr90
  RES T-90 CN 'b'
  MOVE '1' TO EBID
  AS
/*Selects eddy bars from yr73
  RES T-73 CN 'b'
  MOVE '1' TO EBID
  AS
/*Selects eddy bars from yr65
  RES T-65 CN 'b'
  MOVE '1' TO EBID
  AS
/*Selects eddy bars from yr52a
  RES T-S52 CN 'b'
  MOVE '1' TO EBID
  AS
/*Selects eddy bars from yr52b
  RES T-O52 CN 'b'
  MOVE '1' TO EBID
  AS
/*Selects eddy bars from yr35
  RES T-35 CN 'b'
  MOVE '1' TO EBID
  AS
```

```
/*finish
  Q STOP
&end

/*Gets rid of everything but EBID
dissolve zztemp9 %output% ebid poly
kill zztemp1 all
kill zztemp2 all
kill zztemp3 all
kill zztemp4 all
kill zztemp5 all
kill zztemp6 all
kill zztemp7 all
kill zztemp8 all
kill zztemp9 all

&return
```

APPENDIX C- AML used to calculate areas of significant erosion and deposition

```
&args year1cv year2cv output year1 year2
/*Program to calculate change from year1 to year2 with year1 being the earlier year
/*Direct comparison--does NOT adjust for discharge differences
/*Designed for pre- to post 1996 flood comparison for Reach between Lees Ferry to
Badger

/*Checks for proper command line entry
&if ^ [exists %year1cv% -cover] &then &do
  &type %year1cv% does not exist...
  &type Usage:  &r pg-ch-dir2 <First year cover> <Second year cover> <output cover>
  &type                 <First year number> <Second year number>
  &return
&end
&if ^ [exists %year2cv% -cover] &then &do
  &type %year2cv% does not exist...
  &type Usage:  &r pg-ch-dir2 <First year cover> <Second year cover> <output cover>
  &type                 <First year number> <Second year number>
  &return
&end

/*Places files together for analysis
union %year1cv% %year2cv% zztemp3 .000001 join

/*Adds new attributes for computing change
additem zztemp3.pat zztemp3.pat change 25 25 c
additem zztemp3.pat zztemp3.pat path 25 25 c

/*Computes change
&data arc info
  ARC
  SEL ZZTEMP3.PAT
  MOVE 'missed' TO CHANGE
  MOVE 'missed' TO PATH
  AS
/*To show areas not mapped
  RES L-PRE CN ''
  MOVE 'nm-pre' TO CHANGE
  MOVE 'nm-pre' TO PATH
  AS
  RES L-APOST CN ''
  MOVE 'nm-post' TO CHANGE
  MOVE 'nm-post' TO PATH
  AS
/*To show river
```

```
  RES L-PRE CN 'riv' OR  L-APOST CN 'riv'
  MOVE 'river' TO CHANGE
  MOVE 'riv-pre-post' TO PATH
  AS
/*No Change for coarse deposits
/*df
  RES T-PRE CN 'df' AND T-APOST CN 'df'
  MOVE 'nc' TO CHANGE
  MOVE 'coarse-coarse' TO PATH
  AS
  RES T-PRE CN 'df' AND T-APOST CN 'gv'
  MOVE 'nc' TO CHANGE
  MOVE 'coarse-coarse' TO PATH
  AS
  RES T-PRE CN 'df' AND T-APOST CN 'talus'
  MOVE 'nc' TO CHANGE
  MOVE 'coarse-coarse' TO PATH
  AS
  RES T-PRE CN 'df' AND T-APOST CN 'rock'
  MOVE 'nc' TO CHANGE
  MOVE 'coarse-coarse' TO PATH
  AS
/*gv
  RES T-PRE CN 'gv' AND T-APOST CN 'df'
  MOVE 'nc' TO CHANGE
  MOVE 'coarse-coarse' TO PATH
  AS
  RES T-PRE CN 'gv' AND T-APOST CN 'gv'
  MOVE 'nc' TO CHANGE
  MOVE 'coarse-coarse' TO PATH
  AS
  RES T-PRE CN 'gv' AND T-APOST CN 'talus'
  MOVE 'nc' TO CHANGE
  MOVE 'coarse-coarse' TO PATH
  AS
  RES T-PRE CN 'gv' AND T-APOST CN 'rock'
  MOVE 'nc' TO CHANGE
  MOVE 'coarse-coarse' TO PATH
  AS
/*talus
  RES T-PRE CN 'talus' AND T-APOST CN 'df'
  MOVE 'nc' TO CHANGE
  MOVE 'coarse-coarse' TO PATH
  AS
  RES T-PRE CN 'talus' AND T-APOST CN 'gv'
  MOVE 'nc' TO CHANGE
```

```
  MOVE 'coarse-coarse' TO PATH
  AS
  RES T-PRE CN 'talus' AND T-APOST CN 'talus'
  MOVE 'nc' TO CHANGE
  MOVE 'coarse-coarse' TO PATH
  AS
  RES T-PRE CN 'talus' AND T-APOST CN 'rock'
  MOVE 'nc' TO CHANGE
  MOVE 'coarse-coarse' TO PATH
  AS
/*rock
  RES T-PRE CN 'rock' AND T-APOST CN 'df'
  MOVE 'nc' TO CHANGE
  MOVE 'coarse-coarse' TO PATH
  AS
  RES T-PRE CN 'rock' AND T-APOST CN 'gv'
  MOVE 'nc' TO CHANGE
  MOVE 'coarse-coarse' TO PATH
  AS
  RES T-PRE CN 'rock' AND T-APOST CN 'talus'
  MOVE 'nc' TO CHANGE
  MOVE 'coarse-coarse' TO PATH
  AS
  RES T-PRE CN 'rock' AND T-APOST CN 'rock'
  MOVE 'nc' TO CHANGE
  MOVE 'coarse-coarse' TO PATH
  AS
  RES T-PRE CN 'rock' AND T-APOST CN 'cm'
  MOVE 'nc' TO CHANGE
  MOVE 'rock-sand-error' TO PATH
  AS
  RES T-PRE CN 'rock' AND T-APOST CN 'b'
  MOVE 'nc' TO CHANGE
  MOVE 'rock-sand-error' TO PATH
  AS
/*Changes in Level
/*No Change
  RES L-PRE CN 'htt' AND L-APOST CN 'htt'
  MOVE 'nc' TO CHANGE
  MOVE 'htt-htt' TO PATH
  AS
  RES L-PRE CN 'ht' AND L-APOST CN 'ht'
  MOVE 'nc' TO CHANGE
  MOVE 'ht-ht' TO PATH
  AS
  RES L-PRE CN 'fs' AND L-APOST CN 'fs'
```

```
  MOVE 'nc' TO CHANGE
  MOVE 'fs-fs' TO PATH
  AS
  RES L-PRE CN 'hf' AND L-APOST CN 'hf'
  MOVE 'nc' TO CHANGE
  MOVE 'hf-hf' TO PATH
  AS
  RES L-PRE CN 'hf' AND L-APOST CN 'ef'
  MOVE 'nc' TO CHANGE
  MOVE 'hf-ef' TO PATH
  AS
  RES L-PRE CN 'w' AND L-APOST CN 'w'
  MOVE 'nc' TO CHANGE
  MOVE 'w-w' TO PATH
  AS
  RES L-PRE CN 'sub' AND L-APOST CN 'sub'
  MOVE 'nc' TO CHANGE
  MOVE 'sub-sub' TO PATH
  AS
/*erosion
/*high terraces
  RES L-PRE CN 'ht' AND L-APOST CN 'river'
  MOVE 'erosion' TO CHANGE
  MOVE 'hi-low' TO PATH
  AS
  RES L-PRE CN 'ht' AND L-APOST CN 'ff'
  MOVE 'erosion' TO CHANGE
  MOVE 'hi-low' TO PATH
  AS
  RES L-PRE CN 'ht' AND L-APOST CN 'ef'
  MOVE 'erosion' TO CHANGE
  MOVE 'hi-low' TO PATH
/*83 sand
  AS
  RES L-PRE CN 'fs' AND L-APOST CN 'river'
  MOVE 'erosion' TO CHANGE
  MOVE 'fs-riv' TO PATH
  AS
  RES L-PRE CN 'fs' AND L-APOST CN 'ff'
  MOVE 'erosion' TO CHANGE
  MOVE 'fs-ff' TO PATH
  AS
  RES L-PRE CN 'fs' AND L-APOST CN 'ef'
  MOVE 'erosion' TO CHANGE
  MOVE 'fs-ef' TO PATH
  AS
```

```
/*84 sand
  RES L-PRE CN 'hf' AND L-APOST CN 'river'
  MOVE 'erosion' TO CHANGE
  MOVE 'hf-riv' TO PATH
  AS
  RES L-PRE CN 'hf' AND L-APOST CN 'ff'
  MOVE 'erosion' TO CHANGE
  MOVE 'hf-ff' TO PATH
  AS
/*fluctuating flow(wet)
  RES L-PRE CN 'w' AND L-APOST CN 'river'
  MOVE 'erosion' TO CHANGE
  MOVE 'w-river' TO PATH
  AS
  RES L-PRE CN 'w' AND L-APOST CN 'sub'
  MOVE 'erosion' TO CHANGE
  MOVE 'w-sub' TO PATH
  AS
/*fluctuating flow (submerged)
  RES L-PRE CN 'sub' AND L-APOST CN 'river'
  MOVE 'erosion' TO CHANGE
  MOVE 'sub-river' TO PATH
  AS
/*Deposition
/*river
  RES L-PRE CN 'river' AND L-APOST CN 'ff'
  MOVE 'deposition' TO CHANGE
  MOVE 'riv-sand' TO PATH
  AS
  RES L-PRE CN 'river' AND L-APOST CN 'ef'
  MOVE 'deposition' TO CHANGE
  MOVE 'riv-sand' TO PATH
  AS
/*submerged
  RES L-PRE CN 'sub' AND L-APOST CN 'ff'
  MOVE 'deposition' TO CHANGE
  MOVE 'sub-emergent' TO PATH
  AS
  RES L-PRE CN 'sub' AND L-APOST CN 'ef'
  MOVE 'deposition' TO CHANGE
  MOVE 'sub-emergent' TO PATH
  AS
/*wet
  RES L-PRE CN 'w' AND L-APOST CN 'ff'
  MOVE 'deposition' TO CHANGE
  MOVE 'wet-dry' TO PATH
```

```
  AS
  RES L-PRE CN 'w' AND L-APOST CN 'ef'
  MOVE 'deposition' TO CHANGE
  MOVE 'wet-dry' TO PATH
  AS
/*ff
  RES L-PRE CN 'ff' AND L-APOST CN 'ef'
  MOVE 'deposition' TO CHANGE
  MOVE 'ff-ef' TO PATH
  AS
/*leftover ff
  RES L-PRE CN 'ff' AND L-APOST CN 'ff'
  MOVE 'nc' TO CHANGE
  MOVE 'ff-ff' TO PATH
  AS

/*Deposition because of type change
/*df
  RES T-PRE CN 'df' AND T-APOST CN 'cm'
  MOVE 'deposition' TO CHANGE
  MOVE 'sand-on-df' TO PATH
  AS
  RES T-PRE CN 'df' AND T-APOST CN 'b'
  MOVE 'deposition' TO CHANGE
  MOVE 'sand-on-df' TO PATH
  AS
/*gv
  RES T-PRE CN 'gv' AND T-APOST CN 'cm'
  MOVE 'deposition' TO CHANGE
  MOVE 'sand-on-gv' TO PATH
  AS
  RES T-PRE CN 'gv' AND T-APOST CN 'b'
  MOVE 'deposition' TO CHANGE
  MOVE 'sand-on-gv' TO PATH
  AS
/*talus
  RES T-PRE CN 'talus' AND T-APOST CN 'cm'
  MOVE 'deposition' TO CHANGE
  MOVE 'sand-on-talus' TO PATH
  AS
  RES T-PRE CN 'talus' AND T-APOST CN 'b'
  MOVE 'deposition' TO CHANGE
  MOVE 'sand-on-talus' TO PATH
  AS
/*rock
  RES T-PRE CN 'rock' AND T-APOST CN 'cm'
```

```
  MOVE 'deposition' TO CHANGE
  MOVE 'sand-on-rock' TO PATH
  AS
  RES T-PRE CN 'rock' AND T-APOST CN 'b'
  MOVE 'deposition' TO CHANGE
  MOVE 'sand-on-rock' TO PATH
  AS
/*Erosion due to change in type
/*cm
  RES T-PRE CN 'cm' AND T-APOST CN 'df'
  MOVE 'erosion' TO CHANGE
  MOVE 'sand-to-coarse' TO PATH
  AS
  RES T-PRE CN 'cm' AND T-APOST CN 'gv'
  MOVE 'erosion' TO CHANGE
  MOVE 'sand-to-coarse' TO PATH
  AS
  RES T-PRE CN 'cm' AND T-APOST CN 'talus'
  MOVE 'erosion' TO CHANGE
  MOVE 'sand-to-coarse' TO PATH
  AS
  RES T-PRE CN 'cm' AND T-APOST CN 'rock'
  MOVE 'erosion' TO CHANGE
  MOVE 'sand-to-coarse' TO PATH
  AS
/*eb, sb, rb
  RES T-PRE CN 'b' AND T-APOST CN 'df'
  MOVE 'erosion' TO CHANGE
  MOVE 'sand-to-coarse' TO PATH
  AS
  RES T-PRE CN 'b' AND T-APOST CN 'gv'
  MOVE 'erosion' TO CHANGE
  MOVE 'sand-to-coarse' TO PATH
  AS
  RES T-PRE CN 'b' AND T-APOST CN 'talus'
  MOVE 'erosion' TO CHANGE
  MOVE 'sand-to-coarse' TO PATH
  AS
  RES T-PRE CN 'b' AND T-APOST CN 'rock'
  MOVE 'erosion' TO CHANGE
  MOVE 'sand-to-coarse' TO PATH
  AS
/*To ignore changes in coarse deposits
  RES T-PRE CN 'df' AND T-APOST CN 'riv'
  MOVE 'nc' TO CHANGE
  MOVE 'df-river' TO PATH
```

```
  AS
  RES T-PRE CN 'gv' AND T-APOST CN 'riv'
  MOVE 'nc' TO CHANGE
  MOVE 'gv-river' TO PATH
  AS
  RES T-PRE CN 'talus' AND T-APOST CN 'riv'
  MOVE 'nc' TO CHANGE
  MOVE 'tal-river' TO PATH
  AS
  RES T-PRE CN 'rock' AND T-APOST CN 'riv'
  MOVE 'nc' TO CHANGE
  MOVE 'rock-river' TO PATH
  AS
  RES T-PRE CN 'riv' AND T-APOST CN 'df'
  MOVE 'nc' TO CHANGE
  MOVE 'river-df' TO PATH
  AS
  RES T-PRE CN 'riv' AND T-APOST CN 'gv'
  MOVE 'nc' TO CHANGE
  MOVE 'river-gv' TO PATH
  AS
  RES T-PRE CN 'riv' AND T-APOST CN 'talus'
  MOVE 'nc' TO CHANGE
  MOVE 'river-talus' TO PATH
  AS
  RES T-PRE CN 'riv' AND T-APOST CN 'rock'
  MOVE 'nc' TO CHANGE
  MOVE 'river-rock' TO PATH
  AS

/*finish
  RES AREA < 0
  MOVE ' ' TO CHANGE
  AS
  Q STOP
&end

/*Gets rid of everything but change
dissolve zztemp3 zztemp4a change poly
dissolve zztemp3 zztemp4b path poly
union zztemp4a zztemp4b %output% # join
kill zztemp3 all
kill zztemp4a all
kill zztemp4b all

&return
```